

A mechanism for anomalous Hall ferromagnetism in twisted bilayer graphene

Nick Bultinck,^{1,*} Shubhayu Chatterjee,^{1,*} and Michael P. Zaletel^{1,2}

¹*Department of Physics, University of California, Berkeley, CA 94720, USA*

²*Materials Sciences Division, Lawrence Berkeley National Laboratory, Berkeley, California 94720*

Motivated by the recent observation of an anomalous Hall effect in twisted bilayer graphene, we use a lowest Landau level model to understand the origin of the underlying symmetry-broken correlated state. This effective model is rooted in the occurrence of Chern bands which arise due to the coupling between the graphene device and its encapsulating substrate. Our model exhibits a phase transition from a spin-valley polarized insulator to a partial or fully valley unpolarized metal as the bandwidth is increased relative to the interaction strength, consistent with experimental observations. In sharp contrast to standard quantum Hall ferromagnetism, the Chern number structure of the flat bands precludes an instability to an inter-valley coherent phase, but allows for an excitonic vortex lattice at large interaction anisotropy.

Moiré graphene systems are a class of simple van der Waals heterostructures [1] hosting interaction driven low-energy physics, making them an exciting platform to advance our understanding of correlated quantum matter. In twisted bilayer graphene (TBG) with a small twist angle between adjacent layers, interaction effects are enhanced by van Hove singularities coming from 8 nearly flat bands around charge neutrality (CN) in the Moiré- or mini-Brillouin zone (mBZ) [2–21]. Observation of correlated insulating states when 2 or 6 of the 8 TBG flat bands are filled confirms the importance of interactions [22–28].

Recent experiments indicate that certain magic angle graphene devices have large resistance peaks at $\nu = 0, 3$, with the latter featuring an anomalous Hall (AH) effect detected via hysteresis in the Hall conductance as a function of the out-of-plane magnetic field [29]. The Hall conductance is of order e^2/h but not yet quantized. Some have detected an meV-scale gap at CN, and a hysteretic behaviour of the Hall conductance with applied field at $\nu = -1$ [30]. In this work we discuss how the breaking of the 180-degree rotational symmetry (C_{2z}) by a partially aligned hexagonal boron-nitride (h-BN) substrate could explain these observations. A variety of works [31–37] have found that h-BN opens up a band gap at the Dirac points of graphene whose magnitude depends on the graphene / h-BN alignment angle, reaching $\Delta_{AB} \sim 17\text{meV}$ [37] to $\sim 30\text{meV}$ [35, 36] at perfect alignment. Notably, even in seemingly unaligned devices with little or no observable h-BN induced Moiré potential, band gaps of several meV are still observed [36, 37]. In TBG, the substrate can likewise gap out the band Dirac points at the K_{\pm} points of the mBZ, splitting the bands as $8 = 4+4$ to create a gap at CN. We find that for certain sublattice splittings the resulting flat bands have Chern number $C = \pm 1$. This makes the TBG case similar to ABC stacked trilayer graphene, where under an appropriately directed electric field the flat bands have Chern numbers ± 3 [38].

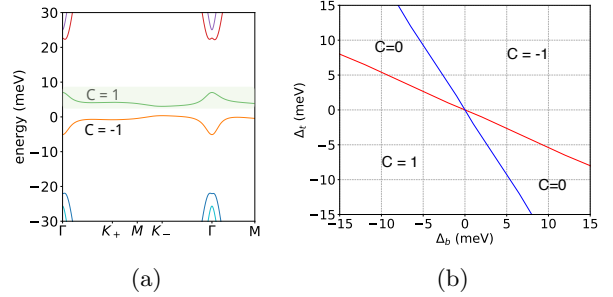


FIG. 1: The effect of sublattice splittings Δ_t and Δ_b on the spinless single-valley Moiré Hamiltonian (SVMH). (a) Band structure around CN for $\Delta_t = 15$ meV and $\Delta_b = 0$. The flat band above (below) CN has Chern number $C = -1$ ($C = 1$). (b) Phase diagram of the SVMH for different Δ_t and Δ_b . Phases are labeled by the Chern number C of the flat $\tau = +$ conduction band. Blue (red) transition lines are characterized by a Dirac cone at the K_- (K_+) point of the mBZ.

Accounting for the C_{2z} -breaking substrate, the basic structure of the problem is as follows. The gap at CN allows us to focus only on the four nearly degenerate conduction (valence) bands for fillings above (below) CN, i.e. $\nu > 0$ ($\nu < 0$). These four Chern bands are uniquely labeled by their valley $\tau = +, -$ and spin $s = \uparrow, \downarrow$; time-reversal switches the valley index and enforces opposite Chern numbers for bands from opposite valleys. Since a $|C| = 1$ band is topologically equivalent to a Landau level (LL), the problem is roughly analogous to a spinful bilayer quantum Hall problem with one flux quanta per unit cell, but with opposite layers (valleys) experiencing opposite magnetic fields. The LLs are degenerate, but as in a quantum Hall ferromagnet (QHFM)[39] at integer filling the electrons may open a gap by spontaneously polarizing into a subset of these LLs, or a coherent superposition of them. In conventional quantum Hall bilayers at filling $\nu = 1$, interactions generically drive inter-layer coherence, e.g., the exciton condensate [40, 41]. But the twist here is the opposing Chern numbers of the two valleys. We find that the Chern number structure provides a topological reason for penalizing a coherent state: an exciton condensate between $C = 1, -1$ bands is analogous

* N.B. and S.C. contributed equally to this work.

to a superconductor in a strong magnetic field, which forces vortices into the order parameter, reducing the gain in the correlation energy. Hence, a spontaneously valley-polarized (VP) state is stable and exhibits AH effect with Hall resistance $\sim h/e^2$ (QAH if completely spin and valley polarized). Further, pinning of valley-polarization by an out-of-plane B^z due to a large orbital g-factor explains the presence of the R_{xy} hysteresis loop observed in Ref. [29].

The possibility of spin and valley polarization and/or quantum anomalous Hall physics and chiral edge states in TBG has been discussed previously in Refs. [38, 42–50], albeit from a different perspective. We also note that a recent self-consistent Hartree-Fock (HF) treatment of the continuum model exhibits *spontaneous* $C_{2z}T$ breaking at CN, though the resulting Chern numbers were $C = \pm 2$ [46].

Substrate-induced Dirac mass and Chern numbers– We model the effect of the h-BN substrate [31] by including in our band calculations a uniform but C_{2z} breaking A-B sublattice splitting Δ_t and Δ_b on the top and bottom layer respectively (see [51] for details). While h-BN may also introduce a Moiré potential, its magnitude falls off much more rapidly with alignment angle than $\Delta_{t/b}$ [37]. For our calculations we used a twist angle $\theta \approx 1.05^\circ$, and have taken a phenomenological corrugation effect into account by using a larger AB/BA inter-layer hopping w_1 as compared to the AA/BB inter-layer hopping w_0 . Taking $w_0/w_1 = 0.85$ results in flat bands separated from the dispersing bands by an energy gap of approximately 20 meV (for zero sublattice splittings).

With sublattice splitting, the phases of the $\tau = +$ valley (or K -valley of monolayer graphene) Moiré Hamiltonian for different parameter regimes of Δ_t and Δ_b are shown in Fig. 1. We find four different regions where both Dirac cones in the mBZ are gapped because of the sublattice splittings. In these regions, there are two isolated flat bands. We find that these four regions have bands with Chern numbers [52] $C = \pm 1$ or $C = 0$, and are separated from each other by a Dirac point at either the K_- or K_+ point in the mBZ. In Fig. 1 we show the Chern number of the flat band for the $\tau = +$ valley above (below) CN in green (orange). The Chern number for the flat bands from the $\tau = -$ valley can be obtained by time-reversal.

The location of the $C = \pm 1$ phases can be understood from the fact that for small $\Delta_t = \Delta_b > 0$ or $\Delta_t = \Delta_b < 0$, the leading order effect of the sublattice potentials is to generate Dirac masses with the same sign at both the K_- and K_+ points of the mBZ. Because both Dirac cones in a single valley have the same chirality, this leads to bands with Chern number ± 1 , a feature earlier work dubbed a “flipped Haldane model” [53] (see also [54–56]). From Fig. 1 we see that even if only one of the layers has a non-zero sublattice splitting, the strong inter-layer coupling ensures that both Dirac cones at the mBZ K -points acquire a mass. These findings can also be inferred analytically within the “chiral” approximation of tBLG

[57, 58], in which all bands are sub-lattice polarized and carry Chern number $C = \sigma\tau$, where σ denotes sublattice.

Metal - valley polarization competition– In this work, we focus only on the four flat *conduction* bands above the CNP (the highlighted band in Fig. 1 and its valley and spin counterparts). In the supplement, we numerically justify this for TBG, showing that $\Delta_t \sim 15$ meV ($\Delta_b = 0$) creates a 30 meV gap between valence and conduction bands [51]. To phenomenologically model the effect of interactions in this set of bands we adopt a lowest Landau level (LLL) description. We can map the Chern bands to a LLL by constructing the Wannier-Qi states [51, 59, 60]. In the following, we use an approximation where the Wannier-Qi states of the flat bands are replaced by the continuum LLL wave functions of a two-dimensional electron gas. Physically, this amounts to neglecting the inhomogeneous Berry curvature in the Chern bands. The AH effect and edge transport reported in Ref. 29 can be explained if there is one VP hole per Moiré unit cell. From the data in Ref. [29] is not possible to exclude a spin-unpolarized, gapless phase. If the spins do polarize however, the underlying mechanism is expected to be the same as in conventional QHFM [39], and is not sensitive to the opposite Chern numbers of the two valleys. Therefore, in the analysis below we ignore spin and focus on the mechanism of valley polarization. Considering the uniform repulsive nature of the projected Coulomb interaction and the numerical evidence against stripes in the LLL [61], we disregard the possibility of interaction-induced charge density waves, and focus on the competition between valley-polarized, inter-valley coherent and metallic phases. For this we need to introduce two parameters in our LLL toy model: the bandwidth and the interaction anisotropy. To achieve a non-zero bandwidth we use a square lattice potential, that sidesteps the complexities of a hexagonal lattice and allows analytical progress.

We consider a torus of length L_x (L_y) in the x (y) direction, with a magnetic field perpendicular to the surface. We choose units in which $L_x L_y = 2\pi N_\phi l_B^2 \equiv N_\phi a^2$, where N_ϕ is the number of flux quanta piercing the torus, and $l_B = (\hbar/eB)^{-1/2}$ is the magnetic length. In particular, we will take $L_x = N_x a$ and $L_y = N_y a$, with $N_\phi = N_x N_y$. Next to the magnetic field, we also add a periodic potential $V_P(x, y) = w(\cos(2\pi x/a) + \cos(2\pi y/a))$, such that there is exactly 2π flux in each unit cell. The potential is invariant under translations over a in both the x and y -direction, which means that the momenta $k_x = n \frac{2\pi}{N_x a}$ and $k_y = n \frac{2\pi}{N_y a}$ ($n \in \mathbb{Z}$) are good quantum numbers.

We are interested in the physics in the LLL with Chern numbers $C = 1, -1$. The electron creation operator projected in these subspaces takes the form $\psi_\pm^\dagger(x, y) = \frac{1}{\sqrt{L_y l_B \sqrt{\pi}}} \sum_k e^{iky - \frac{1}{2i l_B^2} (x \mp k l_B^2)^2} c_{\pm, k}^\dagger$, where we have chosen the Landau gauge which explicitly preserves (continuous) translation symmetry in the y -direction, such that $k = 2\pi n/L_y = 2\pi n/N_y a$ with $n \in \{0, 1, \dots, N_x N_y\}$. We

now proceed in analogy to Ref. 62, and define the Bloch states $c_{\pm, (k_x, k_y)}^\dagger = c_{\pm, \mathbf{k}}^\dagger$ as

$$c_{\pm, \mathbf{k}}^\dagger = \frac{1}{\sqrt{N_x}} \sum_{n=0}^{N_x-1} e^{\pm i k_x (k_y + nQ) l_B^2} c_{\pm, k_y + nQ}^\dagger, \quad (1)$$

where $Q = \sqrt{2\pi}/l_B = 2\pi/a$. The density operator in the LLL $n_{\pm}(\mathbf{q}) = \int d\mathbf{r} e^{-i\mathbf{q}\cdot\mathbf{r}} \psi_{\pm}^\dagger(\mathbf{r}) \psi_{\pm}(\mathbf{r})$ takes the form

$$n_{\pm}(\mathbf{q}) = F(\mathbf{q}) \sum_{k_x, k_y} e^{\pm i q_y k_x l_B^2} c_{\pm, \mathbf{k}-\mathbf{q}/2}^\dagger c_{\pm, \mathbf{k}+\mathbf{q}/2}, \quad (2)$$

where the form factor is given by $F(\mathbf{q}) = e^{-\mathbf{q}^2 l_B^2/4}$. In the Bloch basis, the Hamiltonian term associated with the periodic potential takes the diagonal form $H^p = \sum_{\mathbf{k}} \varepsilon_{\mathbf{k}} (c_{+, \mathbf{k}}^\dagger c_{+, \mathbf{k}} + c_{-, \mathbf{k}}^\dagger c_{-, \mathbf{k}})$, with $\varepsilon_{\mathbf{k}} = -w e^{-\pi/2} [\cos(k_x a) + \cos(k_y a)]$.

We are interested in the effect of density-density interactions on the LLL electrons moving in the periodic potential, described by the following Hamiltonian:

$$H^i = \frac{1}{2N_\phi} \sum_{\mathbf{q}, \tau, \tau'} V_{\tau, \tau'}(\mathbf{q}) : n_{\tau}(\mathbf{q}) n_{\tau'}(-\mathbf{q}), \quad (3)$$

where we neglect the small inter-valley scattering terms [51]. We will consider a general repulsive interaction of the form $V(\mathbf{q}) F^2(\mathbf{q}) = u_0(\mathbf{q})(\mathbb{1} + \tau^x) + u_1(\mathbf{q})(\mathbb{1} - \tau^x)$. In analogy to quantum Hall ferromagnetism [39, 40, 63] and related strongly coupled systems [64, 65], at half-filling of the two bands we expect that the main effect of H^i is to introduce a valley Hund's coupling between the electrons resulting in an insulating ground state. On the other hand, the *kinetic* term H^p coming from the periodic potential favors a metal over the VP insulator. To study the competition between these two phases, we perform a HF analysis using Slater determinants with correlation matrix $\langle c_{\tau, \mathbf{k}}^\dagger c_{\tau', \mathbf{k}'} \rangle = \delta_{\tau, \tau'} \delta_{\mathbf{k}, \mathbf{k}'} \Theta(\varepsilon_F^\tau - \varepsilon_{\mathbf{k}})$, such that $\sum_{\tau} \sum_{\mathbf{k}} \Theta(\varepsilon_F^\tau - \varepsilon_{\mathbf{k}}) = N_\phi$. The possibility of inter-valley coherent states is addressed in the next section. For each Slater determinant, we define the corresponding valley polarization P_v as $P_v = (N_+ - N_-)/N_\phi$, where N_+ (N_-) is the number of electrons in the $+$ ($-$) valley. Without loss of generality, we restrict to $P_v > 0$.

We first consider an isotropic ($u_1(\mathbf{q}) = 0$) dual-gate screened Coulomb potential with LLL form factors $u_0(\mathbf{q}) = 2\pi U e^{-\mathbf{q}^2 l_B^2/2} \tanh(d|\mathbf{q}|)/|\mathbf{q}|$, and screening length $d = a$. Using this interaction potential, we calculated the HF energy E^{HF} [51]. We find that for $W/U \lesssim 0.6$, where $W \equiv 4w e^{-\pi/2}$ is the bandwidth, the completely VP state indeed has the lowest energy. When $W/U \approx 0.6$, the valley polarization P_v of the optimal Slater determinant jumps and starts decreasing continuously, indicating a first-order Mott transition from the VP insulator to an itinerant valley-ferromagnet. Around $W/U \approx 2.0$, P_v continuously goes to zero and a conventional metallic phase sets in [51].

Inter-valley coherence and exciton vortex lattice— In bilayer QH ferromagnets, the insulating layer-polarized

state is unstable to a uniform exciton condensate or inter-layer coherent state in presence of infinitesimal interaction anisotropy $u_1(\mathbf{q}) > 0$ [40]. The situation here is different as even with $u_1(\mathbf{q}) = 0$, there is no SU(2) valley symmetry because of the Chern number mismatch. The VP state therefore only breaks discrete symmetries, indicating there will be no instability of this insulating state. Another, more physical, way to understand the absence of an exciton condensation instability is to use an analogy with type II superconductors. Because electrons in bands with an opposite Chern numbers effectively see opposite magnetic fields, an electron-hole condensate $\Delta(\mathbf{r}) = \langle c_{+, \mathbf{r}}^\dagger c_{-, \mathbf{r}} \rangle$ will behave like a charge $2e$ superconducting order parameter in a perpendicular magnetic field. However, in our scenario a Meissner-like effect, corresponding to uniform amplitude of the exciton order parameter, is ruled out from the outset. Rather, the magnetic field must leak through vortices in the exciton order parameter, leading to an excitonic vortex lattice phase. In this section, we show that both the VP insulator and the unpolarized metal are energetically favorable to the exciton vortex lattice, for sufficiently small interaction anisotropy $u_1(\mathbf{q})$.

For our LLL model, we can derive an exact expression for the exciton vortex lattice order parameter $\Delta(\mathbf{r})$. To respect all symmetries of the square lattice, we expect $\Delta(\mathbf{r})$ to have vortices at both the lattice sites and the plaquette centers, leading to a 4π vorticity in each unit cell. In the analytically tractable limit, we can uniquely determine $\Delta(\mathbf{r})$ up to a translation by demanding its invariance under the magnetic translations $\mathcal{T}(a\hat{x})$ and $\mathcal{T}(\frac{a}{2}(\hat{x} + \hat{y}))$, connecting the anticipated vortices [51]. In Fig. 2 we plot the magnitude of $\Delta(\mathbf{r})$ thus obtained, from which we clearly see the expected Abrikosov vortex lattice. Projecting $\Delta(\mathbf{r})$ to the LLL Bloch basis wavefunctions $\phi_{\pm, \mathbf{k}}(\mathbf{r})$ leads to a diagonal order parameter

$$\Delta_{\mathbf{k}} = \Delta_0 \sum_{j=-\infty}^{\infty} e^{-i\frac{\pi}{2} j^2} e^{-\frac{1}{4}(2k_y + jQ)^2 l_B^2 - ik_x(2k_y + jQ) l_B^2} \quad (4)$$

where Δ_0 represents the overall strength of the exciton condensate. $\Delta_{\mathbf{k}}$ has two nodes with identical phase winding at $\mathbf{k} = \pm(\pi/2, -\pi/2)$, as shown in Fig. 2 [51].

The presence of two zeros in the BZ with the same phase winding is a topological *requirement* for the exciton order parameter, and is not an artifact of our effective LLL model. In an isolated band a with non-zero Chern number C_a , the phase of the electron creation operator $c_{a, \mathbf{k}}^\dagger$ cannot be chosen to be both continuous and single-valued over the BZ. In particular, it must wind $2\pi C_a$ times along the boundary of the BZ in a continuous gauge choice. This implies that the phase of $\Delta_{\mathbf{k}} = \langle c_{+, \mathbf{k}}^\dagger c_{-, \mathbf{k}} \rangle$ winds $2\pi(C_a - C_b) = 4\pi$ times along the BZ boundary for bands from opposite valleys with $C_a = 1$ and $C_b = -1$, which precisely corresponds to winding around two zeros with identical chirality.

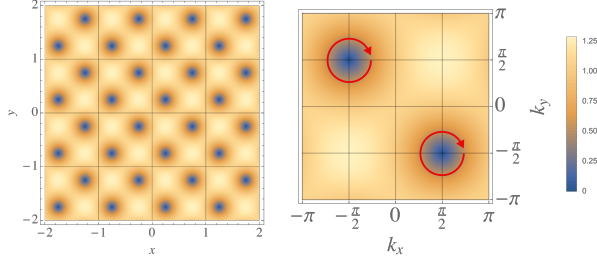


FIG. 2: The magnitude of the excitonic order parameter in real (left) and momentum (right) space (for $a = 1$, $\Delta_0 = 1$). The red circles denote identical phase-winding of $\Delta_{\mathbf{k}}$ at both nodal points.

We now demonstrate that variational states with an exciton vortex lattice have higher energy than the VP state or the metal for small anisotropy u_1 in the interaction H^i . We consider the Slater determinant ground state $|\psi_{MF}\rangle$ of the mean-field Hamiltonian $H_{MF} = \sum_{\mathbf{k}, \tau, \tau'} c_{\mathbf{k}, \tau}^\dagger h_{\tau, \tau'}(\mathbf{k}) c_{\mathbf{k}, \tau'}$, where $h_{\tau, \tau'}(\mathbf{k}) = \epsilon_{\mathbf{k}} \mathbb{1} + h\tau^z + \text{Re}(\Delta_{\mathbf{k}})\tau^x + \text{Im}(\Delta_{\mathbf{k}})\tau^y$. $|\psi_{MF}\rangle$ is characterized by the valley polarization P_v (determined by h) and an exciton vortex lattice of strength Δ_0 , to be treated as variational parameters. The correlation matrix evaluated in this state takes the form of the projector $\langle c_{\tau, \mathbf{k}}^\dagger c_{\tau', \mathbf{k}'} \rangle = P_{\tau, \tau'}(\mathbf{k}) \delta_{\mathbf{k}, \mathbf{k}'}$, which can be used to evaluate the regularized HF energy density $e^{HF}(P_v, \Delta_0)$ of the variational state for a given microscopic interaction at a fixed filling $\nu = 1$. We find that the global minimum of e^{HF} lies at $|P_v| = 1$ and $\Delta_0 = 0$ for the insulator in the limit of flat bands and isotropic interaction ($u_1 = 0$) [51]. We next show that the states of interest, with a fixed valley polarization P_v at filling $\nu = 1$, are stable to the formation of an vortex lattice in presence of small interaction anisotropy. To do this, we consider the difference in energy density $e^{HF}(P_v, \Delta_0) - e^{HF}(P_v, 0)$ perturbatively in $|\Delta_0|$ for arbitrary repulsive interaction parametrized by u_0 and u_1 ; a positive difference would indicate that $\Delta_0 = 0$ corresponds to an energy minimum. For the polarized phase, we find

$$e^{HF}(1, \Delta_0) - e^{HF}(1, 0) = \frac{1}{8h^2} \left[\int_{\mathbf{k}, \mathbf{q}} u_0(\mathbf{q}) |\Delta_+ - \Delta_-|^2 + \int_{\mathbf{k}, \mathbf{q}} u_1(\mathbf{q}) |\Delta_+ + \Delta_-|^2 - 4u_1(\mathbf{0}) \int_{\mathbf{k}} |\Delta_{\mathbf{k}}|^2 \right], \quad (5)$$

where $\Delta_{\pm} \equiv \Delta_{\mathbf{k} \pm \mathbf{q}/2}$ [51]. For a uniform exciton condensate, $\Delta_{\mathbf{k}} = \Delta_0$ and this energy difference is negative [51]. However, for an exciton order parameter formed with electrons and holes from opposite Chern bands, $\nabla_{\mathbf{k}} \Delta_{\mathbf{k}} \neq 0$. Therefore, when u_1 is sufficiently small compared to u_0 the energy of the state with non-zero $\Delta_{\mathbf{k}}$ is higher. So the VP state with $\Delta_0 = 0$, previously shown to be the ground state with an isotropic interaction for small W/u_0 , is indeed robust to small interaction anisotropy. Analogous computations [51] show that the unpolarized metal ($P_v = 0 = \Delta_0$) is stable to the vortex lattice as well. An approximate phase diagram of

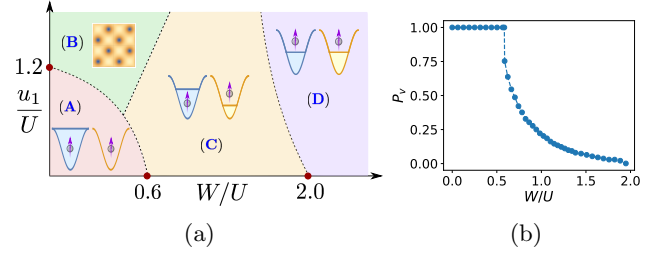


FIG. 3: (a) Approximate phase diagram of spin-polarized interacting electrons from opposite valleys in $C = \pm 1$ bands. The phases are (A) fully VP insulator, (B) exciton vortex lattice, (C) partially polarized metal or itinerant valley-ferromagnet, and (D) unpolarized metal. Everywhere within phases A and C, $R_{xy} \neq 0$. (b) Metal-insulator competition and the valley polarization P_v for isotropic interaction.

our model for a short-range (LLL-projected) interaction anisotropy $u_1(\mathbf{q}) = u_1 e^{-\mathbf{q}^2 l_B^2/2}$ is presented in Fig. 3. For TBG, we expect $W/U \lesssim 0.2$ from the ratio of the bandwidth to the Coulomb interaction, and the anisotropy $u_1/U \lesssim 0.01$ to be small [51, 66], indicating a VP phase consistent with experiments [29, 67]. In the supplement, we numerically solve the mean-field equations for TBG on hBN at $\nu = 3$ and confirm that the spin and VP QAH state is indeed the ground state.

Valley Zeeman effect– Having argued in favor of a VP state at $\nu = 3$, we turn to the observed hysteresis in the $\nu = 3$ Hall conductance as a function of out-of-plane magnetic field B^z [29]. To this end, we compute the orbital g_v -factor for the TBG conduction bands. In a band τ without time-reversal electrons can carry a momentum-dependent orbital moment $m_{\tau, \mathbf{k}}$ [68, 69]. Time-reversal ensures that $m_{\tau, \mathbf{k}} = -m_{-\tau, -\mathbf{k}}$, which averaged over the mBZ produces a valley-Zeeman splitting $E = -g_v \frac{\tau^z}{2} \mu_B B^z$. We find that for $\Delta_b = 0$, $\Delta_t \sim 10 - 30$ meV, g_v ranges from approximately -2 to -6 [51]. Note that for $B^z > 0$, the $C = 1$ band comes down in energy. The sign of this effect is in agreement with the Landau fans of Refs. [29, 67].

Conclusion– We showed that broken inversion symmetry in TBG due to substrate (h-BN) coupling leads to two Chern bands per valley. Spontaneous polarization of holes in spin and valley space then leads to an AH state at $\nu = 3$. Using a LLL model, a HF analysis establishes a stable VP state as the ground state when the bandwidth is small compared to the interaction strength. The opposite Chern numbers for the two valleys precludes uniform inter-valley coherence. The resultant exciton vortex lattice structure reduces correlation energy gain and stabilizes valley-polarization. This result agrees with numerical work on a Hubbard model [70].

Note added– Recently, a quantized AHE with net Chern number $C = 1$ has been observed for a gapped insulator at $\nu = 3$ in TBG aligned with h-BN [67], consistent with our theoretical results. Quantized AHE arising from valley-Chern bands have also been observed [71] and proposed [72, 73] in other Moiré heterostructures, in

accordance with our phenomenological picture of interaction in nearly flat bands with opposite Chern numbers.

Acknowledgements— We thank Aaron Sharpe, Eli Fox and David Goldhaber-Gordon for discussions about their data and sharing their insights. We also thank Ryan Mishmash for explaining the details of Ref. 62 to two of us (SC and NB), and Ehud Altman, Senthil Todadri

and Andrea Young for inspiring discussions. Our work overlaps with concurrent work by Y. Zhang, D. Mao and T. Senthil [74]. MZ and NB were supported by the DOE, office of Basic Energy Sciences under contract no. DE-AC02-05-CH11231. SC acknowledges support from the ERC synergy grant UQUAM via E. Altman.

-
- [1] A. K. Geim and I. V. Grigorieva, “Van der waals heterostructures,” *Nature* **499**, 419 EP – (2013).
- [2] Rafi Bistritzer and Allan H. MacDonald, “Moiré bands in twisted double-layer graphene,” *Proceedings of the National Academy of Sciences* **108**, 12233–12237 (2011).
- [3] E. J. Mele, “Commensuration and interlayer coherence in twisted bilayer graphene,” *Phys. Rev. B* **81**, 161405 (2010).
- [4] J. M. B. Lopes dos Santos, N. M. R. Peres, and A. H. Castro Neto, “Continuum model of the twisted graphene bilayer,” *Phys. Rev. B* **86**, 155449 (2012).
- [5] J. M. B. Lopes dos Santos, N. M. R. Peres, and A. H. Castro Neto, “Graphene bilayer with a twist: Electronic structure,” *Phys. Rev. Lett.* **99**, 256802 (2007).
- [6] G. Trambly de Laissardière, D. Mayou, and L. Magaud, “Localization of dirac electrons in rotated graphene bilayers,” *Nano Letters*, *Nano Letters* **10**, 804–808 (2010).
- [7] S. Shallcross, S. Sharma, E. Kandelaki, and O. A. Pankratov, “Electronic structure of turbostratic graphene,” *Phys. Rev. B* **81**, 165105 (2010).
- [8] E. Suárez Morell, J. D. Correa, P. Vargas, M. Pacheco, and Z. Barticevic, “Flat bands in slightly twisted bilayer graphene: Tight-binding calculations,” *Phys. Rev. B* **82**, 121407 (2010).
- [9] Pilkyung Moon and Mikito Koshino, “Energy spectrum and quantum hall effect in twisted bilayer graphene,” *Phys. Rev. B* **85**, 195458 (2012).
- [10] Guohong Li, A. Luican, J. M. B. Lopes dos Santos, A. H. Castro Neto, A. Reina, J. Kong, and E. Y. Andrei, “Observation of van hove singularities in twisted graphene layers,” *Nature Physics* **6**, 109 EP – (2009).
- [11] A. Luican, Guohong Li, A. Reina, J. Kong, R. R. Nair, K. S. Novoselov, A. K. Geim, and E. Y. Andrei, “Single-layer behavior and its breakdown in twisted graphene layers,” *Phys. Rev. Lett.* **106**, 126802 (2011).
- [12] Wei Yan, Mengxi Liu, Rui-Fen Dou, Lan Meng, Lei Feng, Zhao-Dong Chu, Yanfeng Zhang, Zhongfan Liu, Jia-Cai Nie, and Lin He, “Angle-dependent van hove singularities in a slightly twisted graphene bilayer,” *Phys. Rev. Lett.* **109**, 126801 (2012).
- [13] I. Brihuega, P. Mallet, H. González-Herrero, G. Trambly de Laissardière, M. M. Ugeda, L. Magaud, J. M. Gómez-Rodríguez, F. Ynduráin, and J.-Y. Veullen, “Unraveling the intrinsic and robust nature of van hove singularities in twisted bilayer graphene by scanning tunneling microscopy and theoretical analysis,” *Phys. Rev. Lett.* **109**, 196802 (2012).
- [14] Taisuke Ohta, Jeremy T. Robinson, Peter J. Feibelman, Aaron Bostwick, Eli Rotenberg, and Thomas E. Beechem, “Evidence for interlayer coupling and moiré periodic potentials in twisted bilayer graphene,” *Phys. Rev. Lett.* **109**, 186807 (2012).
- [15] Robin W. Havener, Yufeng Liang, Lola Brown, Li Yang, and Jiwoong Park, “Van hove singularities and excitonic effects in the optical conductivity of twisted bilayer graphene,” *Nano Letters* **14**, 3353–3357 (2014), pMID: 24798502, <https://doi.org/10.1021/nl500823k>.
- [16] R. de Gail, M. O. Goerbig, F. Guinea, G. Montambaux, and A. H. Castro Neto, “Topologically protected zero modes in twisted bilayer graphene,” *Phys. Rev. B* **84**, 045436 (2011).
- [17] Kazuyuki Uchida, Shinnosuke Furuya, Jun-Ichi Iwata, and Atsushi Oshiyama, “Atomic corrugation and electron localization due to moiré patterns in twisted bilayer graphenes,” *Phys. Rev. B* **90**, 155451 (2014).
- [18] A. O. Sboychakov, A. L. Rakhmanov, A. V. Rozhkov, and Franco Nori, “Electronic spectrum of twisted bilayer graphene,” *Phys. Rev. B* **92**, 075402 (2015).
- [19] Jeil Jung, Arnaud Raoux, Zhenhua Qiao, and A. H. MacDonald, “Ab initio theory of moiré superlattice bands in layered two-dimensional materials,” *Phys. Rev. B* **89**, 205414 (2014).
- [20] Dillon Wong, Yang Wang, Jeil Jung, Sergio Pezzini, Ashley M. DaSilva, Hsin-Zon Tsai, Han Sae Jung, Ramin Khajeh, Youngkyou Kim, Juwon Lee, Salman Kahn, Sajjad Tollabimazraehno, Haider Rasool, Kenji Watanabe, Takashi Taniguchi, Alex Zettl, Shaffique Adam, Allan H. MacDonald, and Michael F. Crommie, “Local spectroscopy of moiré-induced electronic structure in gate-tunable twisted bilayer graphene,” *Phys. Rev. B* **92**, 155409 (2015).
- [21] Shiang Fang and Efthimios Kaxiras, “Electronic structure theory of weakly interacting bilayers,” *Phys. Rev. B* **93**, 235153 (2016).
- [22] Y. Cao, J. Y. Luo, V. Fatemi, S. Fang, J. D. Sanchez-Yamagishi, K. Watanabe, T. Taniguchi, E. Kaxiras, and P. Jarillo-Herrero, “Superlattice-induced insulating states and valley-protected orbits in twisted bilayer graphene,” *Phys. Rev. Lett.* **117**, 116804 (2016).
- [23] Kyoungwan Kim, Ashley DaSilva, Shengqiang Huang, Babak Fallahazad, Stefano Larentis, Takashi Taniguchi, Kenji Watanabe, Brian J. LeRoy, Allan H. MacDonald, and Emanuel Tutuc, “Tunable moiré bands and strong correlations in small-twist-angle bilayer graphene,” *Proceedings of the National Academy of Sciences* **114**, 3364–3369 (2017).
- [24] Yuan Cao, Valla Fatemi, Ahmet Demir, Shiang Fang, Spencer L. Tomarken, Jason Y. Luo, Javier D. Sanchez-Yamagishi, Kenji Watanabe, Takashi Taniguchi, Efthimios Kaxiras, Ray C. Ashoori, and Pablo Jarillo-Herrero, “Correlated insulator behaviour at half-filling in magic-angle graphene superlattices,” *Nature* **556**, 80 EP – (2018).
- [25] Matthew Yankowitz, Shaowen Chen, Hryhoriy Pol-

- shyn, K. Watanabe, T. Taniguchi, David Graf, Andrea F. Young, and Cory R. Dean, “Tuning superconductivity in twisted bilayer graphene,” arXiv e-prints , arXiv:1808.07865 (2018), arXiv:1808.07865 [cond-mat.mes-hall].
- [26] Alexander Kerelsky, Leo McGilly, Dante M. Kennes, Lede Xian, Matthew Yankowitz, Shaowen Chen, K. Watanabe, T. Taniguchi, James Hone, Cory Dean, Angel Rubio, and Abhay N. Pasupathy, “Magic Angle Spectroscopy,” arXiv e-prints , arXiv:1812.08776 (2018), arXiv:1812.08776 [cond-mat.mes-hall].
- [27] Youngjoon Choi, Jeannette Kemmer, Yang Peng, Alex Thomson, Harpreet Arora, Robert Polski, Yiran Zhang, Hechen Ren, Jason Alicea, Gil Refael, Felix von Oppen, Kenji Watanabe, Takashi Taniguchi, and Stevan Nadj-Perge, “Imaging Electronic Correlations in Twisted Bilayer Graphene near the Magic Angle,” arXiv e-prints , arXiv:1901.02997 (2019), arXiv:1901.02997 [cond-mat.mes-hall].
- [28] Guorui Chen, Lili Jiang, Shuang Wu, Bosai Lv, Hongyuan Li, Kenji Watanabe, Takashi Taniguchi, Zhiwen Shi, Yuanbo Zhang, and Feng Wang, “Gate-Tunable Mott Insulator in Trilayer Graphene-Boron Nitride Moiré Superlattice,” arXiv e-prints , arXiv:1803.01985 (2018), arXiv:1803.01985 [cond-mat.mes-hall].
- [29] Aaron L. Sharpe, Eli J. Fox, Arthur W. Barnard, Joe Finney, Kenji Watanabe, Takashi Taniguchi, M. A. Kastner, and David Goldhaber-Gordon, “Emergent ferromagnetism near three-quarters filling in twisted bilayer graphene,” arXiv e-prints , arXiv:1901.03520 (2019), arXiv:1901.03520 [cond-mat.mes-hall].
- [30] D. Efetov, “Cascade of superconducting domes and magnetic order around quarter filling in magic angle bilayer graphene,” KITP program “Correlations in Moire Flat Bands” (2019).
- [31] Jeil Jung, Ashley M. DaSilva, Allan H. MacDonald, and Shaffique Adam, “Origin of band gaps in graphene on hexagonal boron nitride,” *Nature Communications* **6**, 6308 EP – (2015).
- [32] B. Hunt, J. D. Sanchez-Yamagishi, A. F. Young, M. Yankowitz, B. J. LeRoy, K. Watanabe, T. Taniguchi, P. Moon, M. Koshino, P. Jarillo-Herrero, and R. C. Ashoori, “Massive Dirac Fermions and Hofstadter Butterfly in a van der Waals Heterostructure,” *Science* **340**, 1427–1430 (2013), arXiv:1303.6942 [cond-mat.mes-hall].
- [33] F. Amet, J. R. Williams, K. Watanabe, T. Taniguchi, and D. Goldhaber-Gordon, “Insulating Behavior at the Neutrality Point in Single-Layer Graphene,” *Phys. Rev. Lett.* **110**, 216601 (2013), arXiv:1209.6364 [cond-mat.mes-hall].
- [34] Menyong Lee, John R. Wallbank, Patrick Gallagher, Kenji Watanabe, Takashi Taniguchi, Vladimir I. Fal’ko, and David Goldhaber-Gordon, “Ballistic miniband conduction in a graphene superlattice,” *Science* **353**, 1526–1529 (2016), arXiv:1603.01260 [cond-mat.mes-hall].
- [35] Matthew Yankowitz, Jeil Jung, Evan Laksono, Nicolas Leconte, Bheema L. Chittari, K. Watanabe, T. Taniguchi, Shaffique Adam, David Graf, and Cory R. Dean, “Dynamic band-structure tuning of graphene moiré superlattices with pressure,” *Nature (London)* **557**, 404–408 (2018), arXiv:1707.09054 [cond-mat.mes-hall].
- [36] A. A. Zibrov, E. M. Spanton, H. Zhou, C. Kometter, T. Taniguchi, K. Watanabe, and A. F. Young, “Even-denominator fractional quantum Hall states at an isospin transition in monolayer graphene,” *Nature Physics* **14**, 930–935 (2018), arXiv:1712.01968 [cond-mat.str-el].
- [37] Hakseong Kim, Nicolas Leconte, Bheema L. Chittari, Kenji Watanabe, Takashi Taniguchi, Allan H. MacDonald, Jeil Jung, and Suyong Jung, “Accurate Gap Determination in Monolayer and Bilayer Graphene/h-BN Moiré Superlattices,” *Nano Letters* **18**, 7732–7741 (2018), arXiv:1808.06633 [cond-mat.mes-hall].
- [38] Ya-Hui Zhang, Dan Mao, Yuan Cao, Pablo Jarillo-Herrero, and T. Senthil, “Nearly Flat Chern Bands in Moiré Superlattices,” arXiv e-prints , arXiv:1805.08232 (2018), arXiv:1805.08232 [cond-mat.str-el].
- [39] S. L. Sondhi, A. Karlhede, S. A. Kivelson, and E. H. Rezayi, “Skyrmions and the crossover from the integer to fractional quantum hall effect at small zeeman energies,” *Phys. Rev. B* **47**, 16419–16426 (1993).
- [40] J.P. Eisenstein, “Exciton condensation in bilayer quantum hall systems,” *Annual Review of Condensed Matter Physics* **5**, 159–181 (2014).
- [41] E. Tutuc, M. Shayegan, and D. A. Huse, “Counterflow Measurements in Strongly Correlated GaAs Hole Bilayers: Evidence for Electron-Hole Pairing,” *Phys. Rev. Lett.* **93**, 036802 (2004), arXiv:cond-mat/0402186 [cond-mat.mes-hall].
- [42] J. F. Dodaro, S. A. Kivelson, Y. Schattner, X. Q. Sun, and C. Wang, “Phases of a phenomenological model of twisted bilayer graphene,” *Phys. Rev. B* **98**, 075154 (2018).
- [43] Alex Thomson, Shubhayu Chatterjee, Subir Sachdev, and Mathias S. Scheurer, “Triangular antiferromagnetism on the honeycomb lattice of twisted bilayer graphene,” *Phys. Rev. B* **98**, 075109 (2018).
- [44] Jian Kang and Oskar Vafek, “Strong coupling phases of partially filled twisted bilayer graphene narrow bands,” arXiv e-prints , arXiv:1810.08642 (2018), arXiv:1810.08642 [cond-mat.str-el].
- [45] Masayuki Ochi, Mikito Koshino, and Kazuhiko Kuroki, “Possible correlated insulating states in magic-angle twisted bilayer graphene under strongly competing interactions,” *Phys. Rev. B* **98**, 081102 (2018).
- [46] Ming Xie and Allan H. MacDonald, “On the nature of the correlated insulator states in twisted bilayer graphene,” arXiv e-prints , arXiv:1812.04213 (2018), arXiv:1812.04213 [cond-mat.str-el].
- [47] Cenke Xu and Leon Balents, “Topological superconductivity in twisted multilayer graphene,” *Phys. Rev. Lett.* **121**, 087001 (2018).
- [48] Yu-Ping Lin and Rahul M. Nandkishore, “A chiral twist on the high- T_c phase diagram in Moiré heterostructures,” arXiv e-prints , arXiv:1901.00500 (2019), arXiv:1901.00500 [cond-mat.str-el].
- [49] Jianpeng Liu, Junwei Liu, and Xi Dai, “A complete picture for the band topology in twisted bilayer graphene,” arXiv e-prints , arXiv:1810.03103 (2018), arXiv:1810.03103 [cond-mat.mes-hall].
- [50] Ya-Hui Zhang and T. Senthil, “Bridging Hubbard Model Physics and Quantum Hall Physics in Trilayer Graphene/h-BN Moiré superlattice,” arXiv e-prints , arXiv:1809.05110 (2018), arXiv:1809.05110 [cond-mat.str-el].
- [51] See supplementary material, which contains Refs. [75–81].
- [52] Takahiro Fukui, Yasuhiro Hatsugai, and Hiroshi Suzuki,

- “Chern numbers in discretized brillouin zone: Efficient method of computing (spin) hall conductances,” *Journal of the Physical Society of Japan* **74**, 1674–1677 (2005).
- [53] Liujun Zou, Hoi Chun Po, Ashvin Vishwanath, and T. Senthil, “Band structure of twisted bilayer graphene: Emergent symmetries, commensurate approximants, and wannier obstructions,” *Phys. Rev. B* **98**, 085435 (2018).
- [54] Hoi Chun Po, Liujun Zou, Ashvin Vishwanath, and T. Senthil, “Origin of mott insulating behavior and superconductivity in twisted bilayer graphene,” *Phys. Rev. X* **8**, 031089 (2018).
- [55] Hoi Chun Po, Liujun Zou, T. Senthil, and Ashvin Vishwanath, “Faithful Tight-binding Models and Fragile Topology of Magic-angle Bilayer Graphene,” *arXiv e-prints*, arXiv:1808.02482 (2018), arXiv:1808.02482 [cond-mat.str-el].
- [56] Zhida Song, Zhijun Wang, Wujun Shi, Gang Li, Chen Fang, and B. Andrei Bernevig, “All ”Magic Angles” Are ”Stable” Topological,” *arXiv e-prints*, arXiv:1807.10676 (2018), arXiv:1807.10676 [cond-mat.mes-hall].
- [57] P. San-Jose, J. González, and F. Guinea, “Non-abelian gauge potentials in graphene bilayers,” *Phys. Rev. Lett.* **108**, 216802 (2012).
- [58] Grigory Tarnopolsky, Alex J. Kruchkov, and Ashvin Vishwanath, “Origin of Magic Angles in Twisted Bilayer Graphene,” *arXiv e-prints*, arXiv:1808.05250 (2018), arXiv:1808.05250 [cond-mat.str-el].
- [59] Nicola Marzari, Arash A. Mostofi, Jonathan R. Yates, Ivo Souza, and David Vanderbilt, “Maximally localized wannier functions: Theory and applications,” *Rev. Mod. Phys.* **84**, 1419–1475 (2012).
- [60] Xiao-Liang Qi, “Generic wave-function description of fractional quantum anomalous hall states and fractional topological insulators,” *Phys. Rev. Lett.* **107**, 126803 (2011).
- [61] Naokazu Shibata and Daijiro Yoshioka, “Stripe State in the Lowest Landau Level,” *Journal of the Physical Society of Japan* **73**, 1 (2004), arXiv:cond-mat/0311213 [cond-mat.mes-hall].
- [62] Ryan V. Mishmash, A. Yazdani, and Michael P. Zaletel, “Majorana lattices from the quantized Hall limit of a proximitized spin-orbit coupled electron gas,” *arXiv e-prints*, arXiv:1811.05990 (2018), arXiv:1811.05990 [cond-mat.mes-hall].
- [63] Z F Ezawa and G Tsitsishvili, “Quantum hall ferromagnets,” *Reports on Progress in Physics* **72**, 086502 (2009).
- [64] Titus Neupert, Luiz Santos, Shinsei Ryu, Claudio Chamon, and Christopher Mudry, “Topological hubbard model and its high-temperature quantum hall effect,” *Phys. Rev. Lett.* **108**, 046806 (2012).
- [65] Titus Neupert, Luiz Santos, Shinsei Ryu, Claudio Chamon, and Christopher Mudry, “Fractional topological liquids with time-reversal symmetry and their lattice realization,” *Phys. Rev. B* **84**, 165107 (2011).
- [66] Shubhayu Chatterjee, Nick Bultinck, and Michael P Zaletel, “Symmetry breaking and skyrmionic transport in twisted bilayer graphene,” *arXiv preprint* arXiv:1908.00986 (2019).
- [67] M. Serlin, C. L. Tschirhart, H. Polshyn, Y. Zhang, J. Zhu, K. Watanabe, T. Taniguchi, L. Balents, and A. F. Young, “Intrinsic quantized anomalous Hall effect in a moiré heterostructure,” *arXiv e-prints*, arXiv:1907.00261 (2019), arXiv:1907.00261 [cond-mat.str-el].
- [68] Di Xiao, Ming-Che Chang, and Qian Niu, “Berry phase effects on electronic properties,” *Rev. Mod. Phys.* **82**, 1959–2007 (2010).
- [69] Ming-Che Chang and Qian Niu, “Berry phase, hyperorbits, and the hofstadter spectrum: Semiclassical dynamics in magnetic bloch bands,” *Phys. Rev. B* **53**, 7010–7023 (1996).
- [70] Titus Neupert, Luiz Santos, Shinsei Ryu, Claudio Chamon, and Christopher Mudry, “Topological hubbard model and its high-temperature quantum hall effect,” *Phys. Rev. Lett.* **108**, 046806 (2012).
- [71] Guorui Chen, Aaron L. Sharpe, Eli J. Fox, Ya-Hui Zhang, Shaoxin Wang, Lili Jiang, Bosai Lyu, Hongyuan Li, Kenji Watanabe, and Takashi Taniguchi, “Tunable Correlated Chern Insulator and Ferromagnetism in Trilayer Graphene/Boron Nitride Moiré Superlattice,” *arXiv e-prints*, arXiv:1905.06535 (2019), arXiv:1905.06535 [cond-mat.mes-hall].
- [72] Xiaomeng Liu, Zeyu Hao, Eslam Khalaf, Jong Yeon Lee, Kenji Watanabe, Takashi Taniguchi, Ashvin Vishwanath, and Philip Kim, “Spin-polarized Correlated Insulator and Superconductor in Twisted Double Bilayer Graphene,” *arXiv e-prints*, arXiv:1903.08130 (2019), arXiv:1903.08130 [cond-mat.mes-hall].
- [73] Jong Yeon Lee, Eslam Khalaf, Shang Liu, Xiaomeng Liu, Zeyu Hao, Philip Kim, and Ashvin Vishwanath, “Theory of correlated insulating behaviour and spin-triplet superconductivity in twisted double bilayer graphene,” *arXiv e-prints*, arXiv:1903.08685 (2019), arXiv:1903.08685 [cond-mat.str-el].
- [74] Ya-Hui Zhang, Dan Mao, and T. Senthil, “Twisted Bilayer Graphene Aligned with Hexagonal Boron Nitride: Anomalous Hall Effect and a Lattice Model,” *arXiv e-prints*, arXiv:1901.08209 (2019), arXiv:1901.08209 [cond-mat.str-el].
- [75] D J Thouless, “Wannier functions for magnetic subbands,” *Journal of Physics C: Solid State Physics* **17**, L325 (1984).
- [76] R. Resta, “Theory of the electric polarization in crystals,” *Ferroelectrics* **136**, 51–55 (1992).
- [77] R. D. King-Smith and David Vanderbilt, “Theory of polarization of crystalline solids,” *Phys. Rev. B* **47**, 1651–1654 (1993).
- [78] Noah F. Q. Yuan and Liang Fu, “Model for the metal-insulator transition in graphene superlattices and beyond,” *Phys. Rev. B* **98**, 045103 (2018).
- [79] Jian Kang and Oskar Vafek, “Symmetry, maximally localized wannier states, and a low-energy model for twisted bilayer graphene narrow bands,” *Phys. Rev. X* **8**, 031088 (2018).
- [80] Mikito Koshino, Noah F. Q. Yuan, Takashi Koretsune, Masayuki Ochi, Kazuhiko Kuroki, and Liang Fu, “Maximally localized wannier orbitals and the extended hubbard model for twisted bilayer graphene,” *Phys. Rev. X* **8**, 031087 (2018).
- [81] Nick Bultinck, Eslam Khalaf, Shang Liu, Shubhayu Chatterjee, Ashvin Vishwanath, and Michael P. Zaletel, “Ground State and Hidden Symmetry of Magic Angle Graphene at Even Integer Filling,” *arXiv e-prints*, arXiv:1911.02045 (2019), arXiv:1911.02045 [cond-mat.str-el].

SUPPLEMENTARY MATERIAL

CONTENTS

I. Flat bands with sublattice splitting	8
II. Suppression of inter-valley scattering	9
III. Construction of Wannier-Qi states	11
IV. Exciton vortex lattice in the lowest Landau level	12
V. Analytical Hartree-Fock energetics for the lowest Landau level model	14
A. Competition between metal and valley polarized states	15
B. Stability of valley polarized insulator and unpolarized metal to exciton vortex lattice	15
VI. Numerical Hartree-Fock analysis of magic angle graphene	17
VII. Orbital moment and valley-Zeeman effect	19

I. FLAT BANDS WITH SUBLATTICE SPLITTING

As was shown in Ref. [31–33], the h-BN substrate generates a substantial Dirac mass when it is nearly aligned with the graphene sheet. We model this by introducing a C_{2z} symmetry breaking sublattice-staggered potential Δ_t and Δ_b in respectively the top and bottom layer graphene sheet.

For the Moiré Hamiltonian, we consider a commensurate Moiré pattern, obtained from an AA stacked bilayer where the top and bottom graphene layers are rotated relative to each other along an out-of-plane rotation axis centered at a hexagon by an angle θ . This gives a Moiré super lattice with microscopic C_{6z} symmetry, which is found to be a very good approximate low-energy symmetry even for microscopically less symmetric Moiré patterns obtained from different initial stacking alignments or different rotation axis [53]. We choose to work with a commensurate pattern in order to use sharply defined Moiré lattice and reciprocal lattice vectors. However, the relevant properties of the electronic band structure around charge neutrality do not rely on the assumption of commensurability. In figure 4(a) we show the mono-layer graphene Brillouin zone with our convention for the reciprocal lattice basis vectors and the high symmetry points K_+ and K_- .

We now consider following spinless (spin-orbit coupling is negligible) single-valley Moiré Hamiltonian

$$H(\mathbf{k}) = \sum_{\mathbf{g}_1, \mathbf{g}_2} \left(h^{++}(R(\theta/2)(\mathbf{k} + \mathbf{X} + \mathbf{g}_1))\delta_{\mathbf{g}_1, \mathbf{g}_2} + h^{--}(R(-\theta/2)(\mathbf{k} + \mathbf{X} + \mathbf{g}_1))\delta_{\mathbf{g}_1, \mathbf{g}_2} + \sum_{\tilde{\mathbf{g}}} \left[T_{\tilde{\mathbf{g}}}^{+-}\delta_{\mathbf{g}_1, \mathbf{g}_2 + \tilde{\mathbf{g}}} + T_{\tilde{\mathbf{g}}}^{-+}\delta_{\mathbf{g}_1 + \tilde{\mathbf{g}}, \mathbf{g}_2} \right] \right) \quad (6)$$

Here, \mathbf{g}_1 and \mathbf{g}_2 lie on the Moiré reciprocal lattice, $R(\theta)$ is a rotation matrix over angle θ , $h^{++}(\mathbf{k}) = th(\mathbf{k}) + \Delta_t\sigma^z$ ($h^{--}(\mathbf{k}) = th(\mathbf{k}) + \Delta_b\sigma^z$) is the mono-layer graphene Hamiltonian of the top (bottom) layer with hopping strength $t = 2.61$ eV and a sublattice splitting $\Delta_t\sigma^z$ ($\Delta_b\sigma^z$). The mono-layer graphene Hamiltonian is given by

$$h(\mathbf{k}) = \begin{pmatrix} 0 & e^{i\mathbf{k}\cdot\mathbf{R}_A} + e^{i\mathbf{k}\cdot(\mathbf{R}_A - \mathbf{R}_1)} + e^{i\mathbf{k}\cdot(\mathbf{R}_A - \mathbf{R}_2)} \\ e^{-i\mathbf{k}\cdot\mathbf{R}_A} + e^{-i\mathbf{k}\cdot(\mathbf{R}_A - \mathbf{R}_1)} + e^{-i\mathbf{k}\cdot(\mathbf{R}_A - \mathbf{R}_2)} & 0 \end{pmatrix}, \quad (7)$$

where $\mathbf{R}_1, \mathbf{R}_2$ are the graphene Bravais lattice vectors and $\mathbf{R}_A, \mathbf{R}_B$ are the sublattice vectors. \mathbf{X} is the position of the center of the mBZ at the mono-layer K_+ -points as shown in Fig.4(b). In the commensurate case we are considering here, \mathbf{X} lies on the Moiré reciprocal lattice. The inter-layer coupling is given by the matrices

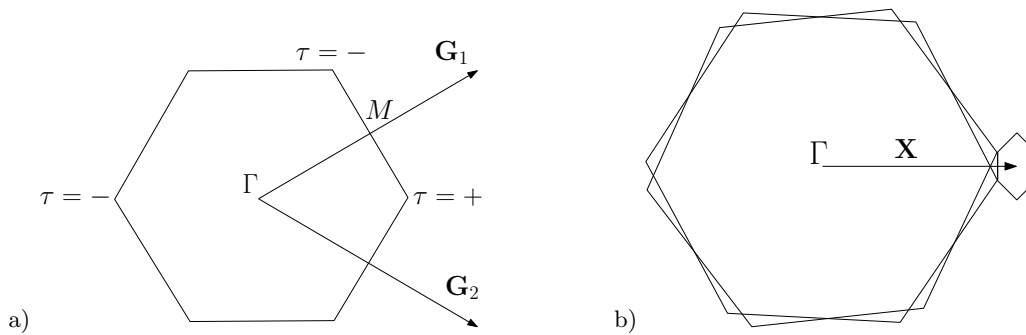


FIG. 4: (a) The mono-layer graphene Brillouin zone with the two basis vectors \mathbf{G}_1 and \mathbf{G}_2 of the reciprocal lattice. We have indicated the high-symmetry K_+ and K_- points, where the Dirac cones are located. (b) The mono-layer Brillouin zones of the top and bottom graphene layer with relative twist angle θ . The vector \mathbf{X} points from the common Γ point of the mono-layer Brillouin zones to the center of the mini-Brillouin zone at the K_+ points.

$$T_{\mathbf{0}} = \begin{pmatrix} w_0 & w_1 \\ w_1 & w_0 \end{pmatrix} \quad (8)$$

$$T_{\mathbf{g}_1} = \begin{pmatrix} w_0 & w_1\omega \\ w_1\omega^* & w_0 \end{pmatrix} \quad (9)$$

$$T_{\mathbf{g}_2} = \begin{pmatrix} w_0 & w_1\omega^* \\ w_1\omega & w_0 \end{pmatrix}, \quad (10)$$

where $\omega = e^{i2\pi/3}$, $\mathbf{g}_1 = (R(\theta/2) - R(-\theta/2))\mathbf{G}_1$ and $\mathbf{g}_2 = (R(\theta/2) - R(-\theta/2))\mathbf{G}_2$. The AB inter-layer hopping strength is $w_1 = 98$ meV. To phenomenologically incorporate the corrugation of the bilayer system we have used an AA-AB inter-layer hopping ratio $w_0/w_1 = 0.85$.

In Fig. 5 we show the resulting flat bands in the mBZ around charge neutrality of the single-valley Moiré Hamiltonian along high-symmetry paths, for different strengths sublattice splittings Δ_t and Δ_b . The twist angle in these calculations was $\theta \approx 1.05^\circ$. When $\Delta_t = \Delta_b = 0$, the flat bands have Dirac cones at K_+ and K_- and are separated from the dispersive bands by an energy gap of approximately 20 meV. If one of the sublattice splittings is non-zero, both Dirac cones acquire a mass because of the strong inter-layer coupling. In Fig. 5 we also show different plots with $\Delta_t = 15$ meV constant and decreasing negative Δ_b to show the two Chern number changing transitions where a Dirac cone occurs at either K_+ or K_- .

II. SUPPRESSION OF INTER-VALLEY SCATTERING

We write the single valley Moiré Hamiltonian schematically as

$$\begin{aligned} H^\tau(\mathbf{k}) &= \sum_{\mathbf{g}_1, \mathbf{g}_2} \sum_{\xi, \sigma, \xi', \sigma'} |\mathbf{k} + \mathbf{g}_1, \xi, \sigma\rangle H_{(\xi, \sigma, \mathbf{g}_1)(\xi', \sigma', \mathbf{g}_2)}^\tau(\mathbf{k}) \langle \mathbf{k} + \mathbf{g}_2, \xi', \sigma' | \\ &= \sum_{\mu} \sum_{\mathbf{g}_1, \mathbf{g}_2} \sum_{\xi, \sigma, \xi', \sigma'} |\mathbf{k} + \mathbf{g}_1, \xi, \sigma\rangle U_{\tau, \mathbf{k}}^\mu(\xi, \sigma, \mathbf{g}_1) \epsilon_\mu^\tau(\mathbf{k}) U_{\tau, \mathbf{k}}^{\mu*}(\xi', \sigma', \mathbf{g}_2) \langle \mathbf{k} + \mathbf{g}_2, \xi', \sigma' |, \end{aligned} \quad (11)$$

where again the vectors \mathbf{g}_i lie on the reciprocal lattice of the Moiré super lattice. Here, we introduced the notation that $\tau \in \{+, -\}$ represents the different Dirac valleys, located at the high symmetry K -points of the mono-layer graphene BZ. The sublattice degree of freedom is denoted by $\sigma \in \{A, B\}$, and the two graphene layers are labeled by $\xi \in \{+, -\}$. The carbon atoms are located at positions \mathbf{r} , such that \mathbf{r} is of the form $\mathbf{r} = R(\xi\theta/2)(m\mathbf{R}_1 + n\mathbf{R}_2 + \mathbf{R}_\sigma)$, where $m, n \in \mathbb{Z}$, $\mathbf{R}_1, \mathbf{R}_2$ are the graphene Bravais lattice vectors and $\mathbf{R}_A, \mathbf{R}_B$ the sublattice vectors.

Importantly, for $H^\tau(\mathbf{k})$ we define the momentum \mathbf{k} relative to the center of the mini-Brillouin zone located at the mono-layer K_τ -points of top and bottom layer. In the second line we diagonalized the Moiré Hamiltonian using the

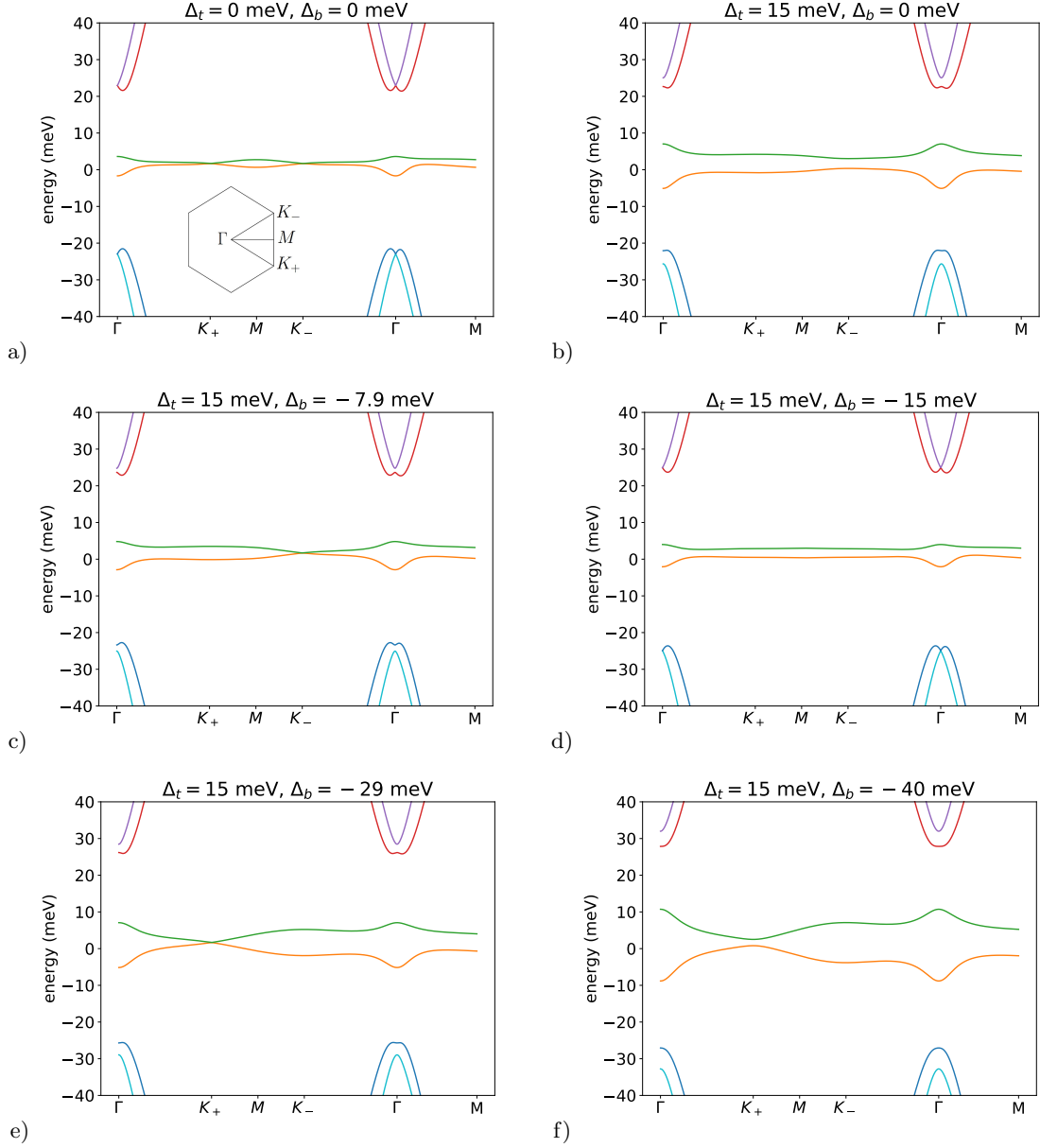


FIG. 5: Flat bands for the single-valley Moiré Hamiltonian at a twist angle $\theta \approx 1.05^\circ$ for different values of the sublattice splittings Δ_t and Δ_b . The intralayer hopping is $t = 2.61$ eV, the AA/BB inter-layer hopping $w_0 = 82$ meV and the AB/BA inter-layer hopping is $w_1 = 98$ meV. (a) Flat bands without sublattice splitting. The high-symmetry paths in the mBZ along which the band spectrum is shown are indicated. There are Dirac cones with small Fermi velocity at the K_+ and K_- points of the mBZ. (b)-(f) Evolution of the flat bands for $\Delta_t = 15$ meV and different values of Δ_b . When Δ_b is zero, a non-zero Δ_t ensures that both Dirac cones acquire a mass. For decreasing negative values of Δ_b , there are two Chern number changing transitions where a Dirac point occurs at either K_+ or K_- .

unitary matrices U . Because we are interested in one band per valley, we drop the μ band index and associate τ with

the band label. In this notation, we write the flat band states in each valley as

$$c_{\mathbf{k},\tau,s}^\dagger = \sum_{\mathbf{g}} \sum_{\xi,\sigma} U_{\tau,\mathbf{k}}(\xi, \sigma, \mathbf{g}) \psi_{\mathbf{k}+\mathbf{g}+\tau\mathbf{K},\xi,\sigma,s}^\dagger \quad (12)$$

$$= \sum_{\mathbf{r}} \sum_{\mathbf{g}} U_{\tau,\mathbf{k}}(\xi, \sigma, \mathbf{g}) e^{i(\mathbf{k}+\mathbf{g}+\tau\mathbf{X})\cdot\mathbf{r}} \psi_{\mathbf{r},s}^\dagger \quad (13)$$

$$\equiv \sum_{\mathbf{r}} \phi_{\tau,\mathbf{k}}([\mathbf{r}]) e^{i(\mathbf{k}+\tau\mathbf{X})\cdot\mathbf{r}} \psi_{\mathbf{r},s}^\dagger \quad (14)$$

$$\equiv \sum_{\mathbf{r}} \tilde{\phi}_{\tau,\mathbf{k}}([\mathbf{r}]) e^{i\mathbf{k}\cdot\mathbf{r}} \psi_{\mathbf{r},s}^\dagger. \quad (15)$$

Here we have introduced the notation $\mathbf{r} = [\mathbf{r}] + \mathbf{t}$, where $[\mathbf{r}]$ is the part of \mathbf{r} lying in the Moire unit cell centered at the origin and \mathbf{t} are Moire lattice vectors. To clarify the notation in going from Eq. (12) to Eq. (13), recall that the position label \mathbf{r} contains the information contained in the labels ξ and σ via the relation $\mathbf{r} = R(\xi\theta/2)(m\mathbf{R}_1 + n\mathbf{R}_2 + \mathbf{R}_\sigma)$. The index s refers to spin. Inverting the above expression now gives us the electron raising operator at position \mathbf{r} projected in the two flat bands:

$$\psi_{\mathbf{r},s}^\dagger = \sum_{\mathbf{k},\tau} e^{-i\mathbf{k}\cdot\mathbf{r}} \tilde{\phi}_{\tau,\mathbf{k}}^*([\mathbf{r}]) c_{\mathbf{k},\tau,s}^\dagger \quad (16)$$

With the projected electron raising operator, which we simply rewrite as $\psi_{\mathbf{t},[\mathbf{r}],s}^\dagger$, we now define

$$n_{[\mathbf{r}]}(\mathbf{q}) = \sum_s \sum_{\mathbf{t}} e^{-i\mathbf{q}\cdot\mathbf{t}} \psi_{\mathbf{t},[\mathbf{r}],s}^\dagger \psi_{\mathbf{t},[\mathbf{r}],s} \quad (17)$$

$$= \sum_s \sum_{\tau,\tau'} \sum_{\mathbf{k}} \phi_{\tau,\mathbf{k}}^*([\mathbf{r}]) \phi_{\tau',\mathbf{k}+\mathbf{q}}([\mathbf{r}]) e^{i(\mathbf{q}+(\tau'-\tau)\mathbf{X})\cdot[\mathbf{r}]} c_{\mathbf{k},\tau,s}^\dagger c_{\mathbf{k}+\mathbf{q},\tau',s} \quad (18)$$

Using the above expression we can write the microscopic Coulomb interaction projected into the flat bands as

$$H^i = \sum_{\mathbf{q}} \sum_{[\mathbf{r}],[\mathbf{r}']} V_{\mathbf{q}}([\mathbf{r}] - [\mathbf{r}']) : n_{[\mathbf{r}]}(\mathbf{q}) n_{[\mathbf{r}]}(-\mathbf{q}) : \quad (19)$$

$$= \sum_{\mathbf{q}} \sum_{s,s'} \sum_{\tau_1,\tau_1',\tau_2,\tau_2'} \sum_{\mathbf{k},\mathbf{k}'} V_{\tau_1,\tau_1',\tau_2,\tau_2'}^{\mathbf{k},\mathbf{k}'}(\mathbf{q}) c_{\mathbf{k},\tau_1,s}^\dagger c_{\mathbf{k}',\tau_2,s'}^\dagger c_{\mathbf{k}'-\mathbf{q},\tau_2',s'} c_{\mathbf{k}+\mathbf{q},\tau_1',s} \quad (20)$$

where

$$V_{\mathbf{q}}([\mathbf{r}] - [\mathbf{r}']) = \sum_{\mathbf{t}} e^{i\mathbf{q}\cdot\mathbf{t}} V(\mathbf{t} + [\mathbf{r}] - [\mathbf{r}']), \quad (21)$$

and $V(\mathbf{r} - \mathbf{r}')$ is the microscopic Coulomb interaction. The projected interaction coefficients are given by

$$V_{\tau_1,\tau_1',\tau_2,\tau_2'}^{\mathbf{k},\mathbf{k}'}([\mathbf{r}],[\mathbf{r}'])(\mathbf{q}) = \sum_{[\mathbf{r}],[\mathbf{r}']} \phi_{\tau_1,\mathbf{k}}^*([\mathbf{r}]) \phi_{\tau_1',\mathbf{k}+\mathbf{q}}([\mathbf{r}]) e^{i(\tau_2'-\tau_2)\mathbf{X}\cdot[\mathbf{r}]} e^{-i\mathbf{q}\cdot([\mathbf{r}]-[\mathbf{r}'])} V_{\mathbf{q}}([\mathbf{r}] - [\mathbf{r}']) \phi_{\tau_2,\mathbf{k}'}^*([\mathbf{r}']) \phi_{\tau_2',\mathbf{k}'-\mathbf{q}}([\mathbf{r}']) e^{i(\tau_1'-\tau_1)\mathbf{X}\cdot[\mathbf{r}']} \quad (22)$$

Now it is important to remember that $\phi_{\tau,\mathbf{k}}(\mathbf{r}) = \sum_{\mathbf{g}} U_{\tau,\mathbf{k}}(\xi, \sigma, \mathbf{g}) e^{i\mathbf{g}\cdot\mathbf{r}}$. Because for the flat band states $U_{\tau,\mathbf{k}}(\xi, \sigma, \mathbf{g})$ decays fast with $|\mathbf{g}|$, $\phi_{\tau,\mathbf{k}}(\mathbf{r})$ varies slowly within the Moiré unit cell. So if $V(\mathbf{r} - \mathbf{r}')$ is sufficiently long-range (like Coulomb), then the sums over $[\mathbf{r}]$ and $[\mathbf{r}']$ will suppress the terms with $\tau_1 \neq \tau_1'$ and $\tau_2 \neq \tau_2'$. For this reason, we restrict to the dominant density-density terms in our effective Landau-level problem.

III. CONSTRUCTION OF WANNIER-QI STATES

Because the single-valley flat bands split by the one-sided staggered potential have Chern number ± 1 , one cannot construct exponentially localized Wannier functions for these bands [75]. However, using the right gauge choice it is possible to construct Wannier functions that are exponentially localized along one direction. Using these quasi-one

dimensional Wannier states there exists a natural mapping from the lattice system to a Landau-level system, as pointed out by Qi in Ref.[60]. Here we review this mapping in the context of TBG.

Consider a system with periodic boundary conditions along two directions, which we refer to as the x and y -directions. Using the flat band states as defined in the previous appendix, we construct the superlattice Wannier-Qi functions as follows:

$$d_{x_0, k_y, \tau, s}^\dagger = \sum_{k_x} e^{-ix_0 k_x} e^{i\alpha_\tau(\mathbf{k})} c_{\mathbf{k}, \tau, s}^\dagger \quad (23)$$

$$= \sum_{\mathbf{r}} \sum_{k_x} e^{i\alpha_\tau(\mathbf{k})} \tilde{\phi}_{\tau, \mathbf{k}}(\mathbf{r}) e^{-ix_0 k_x} e^{i\mathbf{k} \cdot \mathbf{r}} \psi_{\mathbf{r}, s}^\dagger \quad (24)$$

$$= \sum_{[\mathbf{r}]} \sum_{\mathbf{t}'} \left(\sum_{k_x} e^{-i(x_0 - t'_x) k_x} e^{i\alpha_\tau(\mathbf{k})} \tilde{\phi}_{\tau, \mathbf{k}}(\mathbf{r}) \right) e^{ik_y t'_y} \psi_{[\mathbf{r}] + \mathbf{t}', s}^\dagger \quad (25)$$

$$\equiv \sum_{[\mathbf{r}]} \sum_{\mathbf{t}'} W_{\tau, x_0, k_y}(\mathbf{r}) e^{ik_y t'_y} \psi_{\mathbf{r}, s}^\dagger. \quad (26)$$

Here, $e^{i\alpha_\tau(\mathbf{k})}$ ensures an optimal gauge choice such that the functions $W_{\tau, x_0, k_y}(\mathbf{r})$ are exponentially localized in the x -direction around the lattice position x_0 . We now imagine adiabatically threading 2π flux through the hole of the torus, such that the flux is felt by a particle moving on closed path in the y -direction. Because of the Chern number $|C| = 1$, this adiabatic process will change the polarization in the x -direction by one ‘polarization quantum’ [76, 77], which means that the centers of the Wannier functions all shift by one Moire lattice vector along the x -axis (the direction in which they shift depends on the sign of the Chern number). This implies that $W_{\tau, x_0, k_y + g}(\mathbf{r}) = W_{\tau, x_0 + \tau t_x, k_y}(\mathbf{r})$, where g is the norm of the Moiré reciprocal basis vectors. Therefore, we can use $k \equiv k_y + \tau g$ as a single label for our Wannier-Qi states $W_{\tau, k}(\mathbf{k})$ (for each $k_y \in [0, g]$, there is one Wannier function with a particular value for x_0 in each Moiré unit cell). One can now straightforwardly map the Chern band to a LLL, by replacing each Wannier-Qi function $W_{\tau, k}(\mathbf{r})$ by the corresponding LLL Gaussian wave function. One of the main approximations in using the LLL states instead of the Wannier-Qi states of the twisted bilayer is that we ignore any Berry-curvature inhomogeneity.

IV. EXCITON VORTEX LATTICE IN THE LOWEST LANDAU LEVEL

The perpendicular magnetic field seen by the exciton order parameter $\Delta(\mathbf{r}) = \langle c_{+, \mathbf{r}}^\dagger c_{-, \mathbf{r}} \rangle$ induces a vortex lattice in the order parameter. Since $\Delta(\mathbf{r})$ essentially behaves like a charge $q = 2e$ object in a magnetic field, the solution to this vortex lattice may be obtained by solving the Ginzburg Landau (GL) equation for $\Delta(\mathbf{r})$. For analytical tractability, we focus on vortex lattice solution of the linearized GL equation. Our solution is exact only at the upper critical field H_{c2} of the corresponding superconductor, but we expect our results to be valid more generally. In this limit, the problem reduces to the solving the Schrodinger equation for a single particle of charge $2e$. In the Landau gauge $\mathbf{A} = Bx\hat{y}$, this solution is given by

$$\Delta(\mathbf{r}) = \sum_k C_k e^{iky} e^{-\frac{1}{2\xi^2}(x - k\xi^2)^2}, \quad \xi = \frac{l_B}{\sqrt{2}} \quad (27)$$

The exciton vortex lattice we consider has 2π flux through each plaquette of the square lattice of side a , i.e, $a^2 = 2\pi l_B^2$. Since each elementary vortex carries a flux of π , we therefore expect two elementary vortices within a plaquette. Inspired by the computation of similar vortex patterns for the superconducting order parameter in Ref. [62], we choose the vortex lattice wavefunction to be symmetric under magnetic translations $\mathcal{T}_1 = \mathcal{T}(a\hat{y})$ and $\mathcal{T}_2 = \mathcal{T}(\frac{a}{2}(\hat{x} + \hat{y}))$. Note that the magnetic translation operators for a particle of charge q in a magnetic field \mathbf{B} satisfy the following algebra:

$$\mathcal{T}_{\mathbf{R}} \mathcal{T}_{\mathbf{R}'} = e^{iq\mathbf{B} \cdot (\mathbf{R} \times \mathbf{R}') / \hbar} \mathcal{T}_{\mathbf{R}'} \mathcal{T}_{\mathbf{R}} \quad (28)$$

Since $\Delta(\mathbf{r})$ is a charge $q = 2e$ order parameter, we have $q\mathbf{B} \cdot (\mathbf{R}_1 \times \mathbf{R}_2) / \hbar = (2e)B(a^2/2) / \hbar = 2\pi$ implying that \mathcal{T}_1 and \mathcal{T}_2 commute with each other. Being magnetic translation operators, they commute with the free Hamiltonian of a particle of charge q . Since our goal is to express $\Delta(\mathbf{r})$ in the Bloch basis, where the eigenstates of particles with charge $q = e$ are invariant under the square lattice translations $\mathcal{T}_1 = \mathcal{T}(a\hat{y})$ and $\mathcal{T}_3 = \mathcal{T}(a\hat{x})$, we also choose the phases of \mathcal{T}_1 and \mathcal{T}_2 such that $\mathcal{T}_3 = \mathcal{T}_2^2 \mathcal{T}_1^{-1}$ is identically satisfied. Consistent with these conditions, we find that

$$\mathcal{T}_1 = e^{-iap_y / \hbar}; \quad \mathcal{T}_2 = e^{i\pi/2} e^{ia y / l_B^2} e^{-ia(p_x + p_y) / (2\hbar)} \quad (29)$$

Now we impose the magnetic translation symmetry requirements on $\Delta(\mathbf{r})$. For \mathcal{T}_1 , we have

$$\mathcal{T}(a\hat{y})\Delta(\mathbf{r}) = \sum_k C_k e^{-ika} e^{iky} e^{-\frac{1}{2\xi^2}(x-k\xi^2)^2} = \Delta(\mathbf{r}) \implies k = k_j = \frac{2\pi j}{a} = jQ \text{ for } j \in \mathbb{Z} \quad (30)$$

where we have defined $Q = 2\pi/a$. Therefore, we can write

$$\Delta(\mathbf{r}) = \sum_{j=-\infty}^{\infty} C_j e^{ik_j y} e^{-\frac{1}{2\xi^2}(x-k_j\xi^2)^2} \quad (31)$$

For \mathcal{T}_2 , we have, using $2\pi l_B^2 = a^2$ or equivalently $a = Ql_B^2$,

$$\begin{aligned} \mathcal{T}_2\Delta(\mathbf{r}) &= \sum_{j=-\infty}^{\infty} C_j e^{i\pi/2} e^{-ik_j a} e^{i(k_j + a/l_B^2)y} e^{-\frac{1}{2\xi^2}(x-(k_j + a/l_B^2)\xi^2)^2} = \sum_{j=-\infty}^{\infty} C_j e^{i\pi j + i\pi/2} e^{ik_{j+1}y} e^{-\frac{1}{2\xi^2}(x-k_{j+1}\xi^2)^2} \\ &= \Delta(\mathbf{r}) \implies C_j e^{i\pi j + i\pi/2} = C_{j+1} \implies C_j = e^{i\frac{\pi}{2}j^2} C_0 \end{aligned} \quad (32)$$

Therefore, we have the following form of $\Delta(\mathbf{r})$:

$$\Delta(\mathbf{r}) = C_0 \sum_{j=-\infty}^{\infty} e^{i\frac{\pi}{2}j^2} e^{ik_j y} e^{-\frac{1}{2\xi^2}(x-k_j\xi^2)^2} \quad (33)$$

We can now find the projection of $\Delta(\mathbf{r})$ on the single particle Bloch wave-functions. We focus on the lowest Landau level since we are only interested in $C = \pm 1$ bands. We define

$$\Delta_{00}(\mathbf{k}, \mathbf{k}') = \int d\mathbf{r} \Delta(\mathbf{r}) \phi_{+,\mathbf{k}}^*(\mathbf{r}) \phi_{-,\mathbf{k}'}(\mathbf{r}) \quad (34)$$

where $\phi_{\pm,\mathbf{k}}(\mathbf{r})$ are the Bloch wave-functions defined in Eq. (1) in the main text. Given the symmetry of $\Delta(\mathbf{r})$ under magnetic translations \mathcal{T}_1 and \mathcal{T}_3 , we expect it to be diagonal in Bloch space. Indeed, we find that $\Delta_{00}(\mathbf{k}, \mathbf{k}') = \Delta_{\mathbf{k}} \delta_{\mathbf{k}, \mathbf{k}'}$, where

$$\Delta_{\mathbf{k}} = \Delta_0 \sum_{j=-\infty}^{\infty} e^{-i\frac{\pi}{2}j^2} e^{-\frac{1}{4}(2k_y + jQ)^2 l_B^2} e^{-ik_x(2k_y + jQ)l_B^2} \quad (35)$$

where $\Delta_0 = \frac{C_0}{\sqrt{2}}$ is a measure of the overall strength of the exciton vortex lattice order parameter.

We can recast $\Delta_{\mathbf{k}}$ in terms of the Jacobi theta function as follows

$$\begin{aligned} \Delta_{\mathbf{k}} &= \Delta_0 e^{(k_x - ik_y)^2 l_B^2 - k_x^2 l_B^2} \vartheta_3 \left(z = -\frac{k_x - ik_y}{Q}; \tau = \frac{e^{-i\pi/4}}{\sqrt{2}} \right) \\ &\text{with } \vartheta_3(z; \tau) = \sum_{n=-\infty}^{\infty} e^{i\pi\tau n^2 + i2\pi n z}. \end{aligned} \quad (36)$$

The Jacobi theta function has zeros at $z = m + n\tau + 1/2 + \tau/2$, where $m, n \in \mathbb{Z}$. Restricting to the first BZ, we find that $\Delta_{\mathbf{k}} = 0$ at $\mathbf{k} = \pm \mathbf{k}_0$, with $\mathbf{k}_0 = (\pi/2, -\pi/2)$. Further, a power series expansion about the zeros shows that $\Delta_{\pm \mathbf{k}_0 + \mathbf{q}} = \pm A(q_x - iq_y) + O(q^2)$ (for some $A \in \mathbb{C}$), indicating that both nodes have the same chirality. The presence of these two nodes in the BZ, which is a topological requirement of $\Delta_{\mathbf{k}}$ arising from hybridization of bands with $C = \pm 1$, is confirmed by plotting the absolute value of $\Delta_{\mathbf{k}}$ in Fig. 2 in the main text.

The nodes in the exciton order parameter are intimately related to the Dirac cones of the $C_{2z}T$ -symmetric single-valley Moiré Hamiltonian, and the associated Wannier obstruction [53–56, 78–80]. To see this, consider a free fermion Hamiltonian with two bands that are isolated from the other bands, such that the momentum space Hamiltonian projected onto the two isolated bands takes the form

$$\begin{aligned} H(\mathbf{k})|_{+,-} &= (\epsilon_{\mathbf{k}} - \mu)|u_{+,\mathbf{k}}\rangle\langle u_{+,\mathbf{k}}| - (\epsilon_{\mathbf{k}} - \mu)|u_{-,\mathbf{k}}\rangle\langle u_{-,\mathbf{k}}| \\ &\quad + \Delta_{\mathbf{k}}|u_{+,\mathbf{k}}\rangle\langle u_{-,\mathbf{k}}| + \Delta_{\mathbf{k}}^*|u_{-,\mathbf{k}}\rangle\langle u_{+,\mathbf{k}}|, \end{aligned} \quad (37)$$

where $|u_{\pm,\mathbf{k}}\rangle$ are the periodic parts of the Bloch states in the two-band subspace. The dispersion of the two bands is given by $\pm\sqrt{(\epsilon_{\mathbf{k}} - \mu)^2 + |\Delta_{\mathbf{k}}|^2}$ (for simplicity, but without loss of generality, we use a particle-hole symmetric projected Hamiltonian). We consider the situation where $|u_{\pm,\mathbf{k}}\rangle$ has Chern number ± 1 , i.e. $\frac{1}{2\pi} \int_{\mathbf{k}} \nabla \times \mathbf{A}_{\pm} = \pm 1$,

where $\mathbf{A}_\pm = -i\langle u_{\pm,\mathbf{k}}|\nabla|u_{\pm,\mathbf{k}}\rangle$. Using the same reasoning as for the exciton order parameter, and the fact that the Hamiltonian has to be periodic over the Brillouin zone, we conclude that $\Delta_{\mathbf{k}}$ has two zeros in the Brillouin zone around which its phase winds by 2π . Now imagine tuning μ from minus infinity to plus infinity. In this process the Chern number of the lowest energy band changes from $+1$ to -1 , which is only possible if the energy gap between the two bands closes for intermediate values of μ . From the band dispersion, we see that this gap closing will occur precisely at the momenta where the zeros of $\Delta_{\mathbf{k}}$ are located. At these points, the nodes in $\Delta_{\mathbf{k}}$ give rise to Dirac cones with the same chirality.

V. ANALYTICAL HARTREE-FOCK ENERGETICS FOR THE LOWEST LANDAU LEVEL MODEL

In this section, we compute the Hartree-Fock (HF) energy in a variational Slater determinant state for the Hamiltonian $H = H^i + H^p$, which we recall for completeness.

$$\begin{aligned} H^p &= \sum_{\mathbf{k},\tau} \epsilon_{\mathbf{k}} c_{\tau,\mathbf{k}}^\dagger c_{\tau,\mathbf{k}}, \text{ where } \epsilon_{\mathbf{k}} = -\frac{W}{4} \left[\cos\left(\frac{2\pi x}{a}\right) + \cos\left(\frac{2\pi y}{a}\right) \right] \\ H^i &= \frac{1}{2N_\phi} \sum_{\mathbf{q},\tau,\tau'} V_{\tau,\tau'}(\mathbf{q}) : n_\tau(\mathbf{q}) n_{\tau'}(-\mathbf{q}) :, \text{ where } V_{\tau,\tau'}(\mathbf{q}) = u_0(\mathbf{q}) \begin{pmatrix} 1 & 1 \\ 1 & 1 \end{pmatrix} + u_1(\mathbf{q}) \begin{pmatrix} 1 & -1 \\ -1 & 1 \end{pmatrix} \end{aligned} \quad (38)$$

In Eq. (38), $u_0(\mathbf{q})$ is the symmetric part of the interaction, while $u_1(\mathbf{q})$ represents the anisotropy. We evaluate $\langle H \rangle$ for a variational Slater determinant state, which can capture the fully valley polarized Chern insulator, the unpolarized and partially polarized metallic states, and the exciton condensate (both uniform and a vortex lattice) in different limits. Our variational state $|\psi_{MF}\rangle$ may be taken to be the Slater determinant ground state of a mean field Hamiltonian of the form $H_{MF} = \sum_{\mathbf{k},\tau,\tau'} c_{\mathbf{k},\tau}^\dagger h_{\tau,\tau'}(\mathbf{k}) c_{\mathbf{k},\tau'}$, where

$$h_{\tau,\tau'}(\mathbf{k}) = \begin{pmatrix} \epsilon_{\mathbf{k}} + h & \Delta_{\mathbf{k}}^* \\ \Delta_{\mathbf{k}} & \epsilon_{\mathbf{k}} - h \end{pmatrix} \quad (39)$$

Such a state $|\psi_{MF}\rangle$ is characterized by two variational parameters, the polarization P_v (determined by h) and the strength of the excitonic order parameter Δ_0 . In the $|h| \gg \max\{|\epsilon_{\mathbf{k}}|\}$ and $\Delta_{\mathbf{k}} = 0$ limit, our Slater determinant state is thus fully valley polarized with $|P_v| = 1$, while for $h = \Delta_{\mathbf{k}} = 0$ we have an unpolarized metal. For $h \neq 0$ and $\Delta_{\mathbf{k}} = 0$, the state is a partially polarized metal with different chemical potential for the $\tau = \pm$ valleys. For $h = 0$ and $\Delta_{\mathbf{k}} \neq 0$, the state is an excitonic condensate or vortex lattice (depending on the precise structure of $\Delta_{\mathbf{k}}$), with $P_v = 0$ fixed by the discrete $z \rightarrow -z$ symmetry of H_{MF} . The most general state will have both h and $\Delta_{\mathbf{k}}$ non-zero.

Evaluating the covariance matrix for $|\psi_{MF}\rangle$ with a chemical potential μ which fixes the filling of the mean-field bands gives:

$$\begin{aligned} \langle c_{\tau,\mathbf{k}}^\dagger c_{\tau',\mathbf{k}'} \rangle &= P_{\tau,\tau'}(\mathbf{k}) \delta_{\mathbf{k},\mathbf{k}'}, \text{ with } P_{\tau,\tau'}(\mathbf{k}) = \begin{pmatrix} |u_{\mathbf{k}}|^2 \Theta_{\mathbf{k},\alpha} + |v_{\mathbf{k}}|^2 \Theta_{\mathbf{k},\beta} & u_{\mathbf{k}} v_{\mathbf{k}} (\Theta_{\mathbf{k},\alpha} - \Theta_{\mathbf{k},\beta}) \\ u_{\mathbf{k}}^* v_{\mathbf{k}}^* (\Theta_{\mathbf{k},\alpha} - \Theta_{\mathbf{k},\beta}) & |v_{\mathbf{k}}|^2 \Theta_{\mathbf{k},\alpha} + |u_{\mathbf{k}}|^2 \Theta_{\mathbf{k},\beta} \end{pmatrix} \\ \text{where } u_{\mathbf{k}} &= \cos\left(\frac{\theta_{\mathbf{k}}}{2}\right), v_{\mathbf{k}} = e^{i\phi_{\mathbf{k}}} \sin\left(\frac{\theta_{\mathbf{k}}}{2}\right), \tan(\theta_{\mathbf{k}}) = \frac{|\Delta_{\mathbf{k}}|}{h}, e^{i\phi_{\mathbf{k}}} = \frac{\Delta_{\mathbf{k}}}{|\Delta_{\mathbf{k}}|} \text{ and } \Theta_{\mathbf{k},\alpha(\beta)} = \Theta(\mu - E_{\mathbf{k},\alpha(\beta)}) \end{aligned} \quad (40)$$

One can indeed check that $P_{\tau,\tau'}(\mathbf{k})$ is a projector matrix, i.e. $P^2 = P$, as expected for a Slater determinant state. We use these correlators to evaluate $\langle H \rangle$ via Wick's theorem.

$$\lim_{N_\phi \rightarrow \infty} \frac{E^{HF}}{N_\phi} = \frac{1}{2} \int_{\mathbf{k},\mathbf{k}',\mathbf{q}} \sum_{\tau,\tau'} V_{\tau\tau'}^{LL}(\mathbf{q}) \left(P_{\tau,\tau}(\mathbf{k}) P_{\tau',\tau'}(\mathbf{k}') \delta_{\mathbf{q},0} - P_{\tau,\tau'}(\mathbf{k} - \mathbf{q}/2) P_{\tau',\tau}(\mathbf{k} + \mathbf{q}/2) \delta_{\mathbf{k},\mathbf{k}'} \right) + \int_{\mathbf{k}} \epsilon_{\mathbf{k}} \text{Tr}(P(\mathbf{k})) \quad (41)$$

where we have taken the thermodynamic limit, set the lattice spacing $a = 1$ and used the notation $\int_{\mathbf{k}} = \int \frac{d^2k}{(2\pi)^2}$ to denote integration over the first BZ. We now focus on different limits where we can analytically compute the regularized energy density $e^{HF}(P_v, \Delta_0) \equiv \lim_{N_\phi \rightarrow \infty} \left(\frac{E^{HF}}{N_\phi} - \frac{u_0(\mathbf{0})}{2} \right)$ (where we have subtracted the formally infinite self-energy contribution that is canceled by the positive background) and get physical intuition about the phase diagram and stability of the different phases.

A. Competition between metal and valley polarized states

First, we focus on the competition between the metallic state and valley polarized state (setting $\Delta_0 = 0$). The anisotropic part of the interaction $u_1(\mathbf{q})$, while crucial for the excitonic order parameter, does not play a prominent role here other than altering phase boundaries slightly, so we set it to zero for simplicity. In this case, the covariance matrix takes the form

$$\langle c_{\tau,\mathbf{k}}^\dagger c_{\tau'\mathbf{k}'} \rangle = \delta_{\tau,\tau'} \delta_{\mathbf{k},\mathbf{k}'} f_{\mathbf{k}}^\tau, \text{ where } f_{\mathbf{k}}^\tau = \Theta(\varepsilon_F^\tau - \varepsilon_{\mathbf{k}}) \quad (42)$$

with a separate Fermi energy $\varepsilon_F^\tau = \mu + \tau h$ for the two bands ($\tau = \pm 1$). Therefore, the regularized HF energy density is given by

$$e^{HF}(P_v, 0) = -\frac{1}{2} \sum_{\tau} \int_{\mathbf{q}, \mathbf{k}} u_0(\mathbf{q}) f_{\mathbf{k}+\mathbf{q}/2}^\tau f_{\mathbf{k}-\mathbf{q}/2}^\tau + \sum_{\tau} \int_{\mathbf{k}} \varepsilon_{\mathbf{k}} f_{\mathbf{k}}^\tau \quad (43)$$

To intuitively understand the physics, let us consider two extreme limits. For the fully valley polarized state, one of bands is completely full while the other is completely empty. Hence, Eq. (43) evaluates to

$$e^{HF}(1, 0) = -\frac{1}{2} \int u_0(\mathbf{q}) + \int_{\mathbf{k}} \varepsilon_{\mathbf{k}} \quad (44)$$

For the unpolarized metal, $f_{\mathbf{k}}^+ = f_{\mathbf{k}}^- \equiv f_{\mathbf{k}} = \Theta(-\varepsilon_{\mathbf{k}})$. Defining $g(\mathbf{q}) = \int_{\mathbf{k}} f_{\mathbf{k}+\mathbf{q}/2} f_{\mathbf{k}-\mathbf{q}/2}$, Eq. (43) evaluates to

$$e^{HF}(0, 0) = -\frac{1}{2} \int u_0(\mathbf{q}) g(\mathbf{q}) + 2 \int_{\mathbf{k}: \varepsilon_{\mathbf{k}} < 0} \varepsilon_{\mathbf{k}} \quad (45)$$

The function $g(\mathbf{q})$ is proportional to the overlap of the Fermi surface with itself when shifted by \mathbf{q} . Hence, $g(\mathbf{q})$ has a maximum value of 1 at $\mathbf{q} = 0$ and decreases with \mathbf{q} till \mathbf{q} is half a reciprocal lattice vector. Since $u_0(\mathbf{q})$ contains the Landau level projection factor $F^2(\mathbf{q}) = e^{-q^2 l_B^2/2}$, the main contribution to the interaction term comes from $g(\mathbf{q})$ close to zero, which implies that the unpolarized metal has higher energy than the valley polarized state. In other words, interaction favors valley polarization. On the other hand, the kinetic term from the periodic potential favors the metal, as a full dispersing band costs more energy than two half-filled bands.

B. Stability of valley polarized insulator and unpolarized metal to exciton vortex lattice

Following our previous discussion about the metallic phase and the valley polarized insulator, we need to establish that both these phases are stable to an excitonic phase with non-zero $\Delta(\mathbf{r})$ in presence of anisotropy in the interactions ($u_1(\mathbf{q}) \neq 0$). For two $C = +1$ bands, it is well-known that an infinitesimal anisotropy will drive exciton condensation with uniform magnitude. As argued in the main text, our excitonic order parameter $\Delta(\mathbf{r})$ formed which has electrons from the $C = +1$ band and holes from the $C = -1$ band, will behave like a superconducting order parameter in presence of a uniform magnetic field. Therefore, we can rule out a uniform exciton condensate, but an exciton vortex lattice indeed remains a distinct possibility. Below, we argue that such a phase is also energetically more expensive as long as the anisotropy is small enough.

We start off with the fully valley polarized state, corresponding to a large h . We now add a small $\Delta_{\mathbf{k}}$ to see if we gain energy in presence of an arbitrarily weak anisotropy u_1 , while keeping the filling fixed to half. In this limit, the lower (β) band is still full while the upper (α) band is empty, so we can write $\Theta_{\mathbf{k},\alpha} = 0$ and $\Theta_{\mathbf{k},\beta} = 1$. We can write the covariance matrix from Eq. (40) as follows:

$$P_{\tau,\tau'}(\mathbf{k}) = \frac{1}{2} \begin{pmatrix} 1 - \frac{h}{\sqrt{h^2 + |\Delta_{\mathbf{k}}|^2}} & -\frac{\Delta_{\mathbf{k}}}{\sqrt{h^2 + |\Delta_{\mathbf{k}}|^2}} \\ -\frac{\Delta_{\mathbf{k}}^*}{\sqrt{h^2 + |\Delta_{\mathbf{k}}|^2}} & 1 + \frac{h}{\sqrt{h^2 + |\Delta_{\mathbf{k}}|^2}} \end{pmatrix} \quad (46)$$

Using the form of P from Eq. (46) and writing out the terms in Eq. (41) in terms of u_0 and u_1 , we find that (using

$\text{Tr}(P(\mathbf{k})) = 1$):

$$\begin{aligned}
e^{HF}(1, \Delta_0) &= \int_{\mathbf{k}} \varepsilon_{\mathbf{k}} + \frac{1}{2} \left(\int_{\mathbf{k}} \frac{h}{\sqrt{h^2 + |\Delta_{\mathbf{k}}|^2}} \right)^2 u_1(\mathbf{0}) \\
&\quad - \frac{1}{2} \int_{\mathbf{q}, \mathbf{k}} \frac{[u_0(\mathbf{q}) + u_1(\mathbf{q})]}{2} \left(1 + \frac{h^2}{\sqrt{(h^2 + |\Delta_{\mathbf{k}+\mathbf{q}/2}|^2)(h^2 + |\Delta_{\mathbf{k}-\mathbf{q}/2}|^2)}} \right) \\
&\quad - \frac{1}{2} \int_{\mathbf{q}, \mathbf{k}} \frac{[u_0(\mathbf{q}) - u_1(\mathbf{q})]}{4} \frac{(\Delta_{\mathbf{k}-\mathbf{q}/2} \Delta_{\mathbf{k}+\mathbf{q}/2}^* + \Delta_{\mathbf{k}-\mathbf{q}/2}^* \Delta_{\mathbf{k}+\mathbf{q}/2})}{\sqrt{(h^2 + |\Delta_{\mathbf{k}+\mathbf{q}/2}|^2)(h^2 + |\Delta_{\mathbf{k}-\mathbf{q}/2}|^2)}}
\end{aligned} \tag{47}$$

To check the stability perturbatively, we expand in powers of $|\Delta_0|/h$ and consider the difference of energy density $e^{HF}(1, \Delta_0)$ and $e^{HF}(1, 0)$ for the fully polarized state upto quadratic order.

$$e^{HF}(1, \Delta_0) - e^{HF}(1, 0) = \frac{1}{2} \int_{\mathbf{q}, \mathbf{k}} \frac{u_0(\mathbf{q})}{4} \frac{|\Delta_{\mathbf{k}+\mathbf{q}/2} - \Delta_{\mathbf{k}-\mathbf{q}/2}|^2}{h^2} + \frac{1}{2} \int_{\mathbf{q}, \mathbf{k}} \frac{u_1(\mathbf{q})}{4} \frac{|\Delta_{\mathbf{k}+\mathbf{q}/2} + \Delta_{\mathbf{k}-\mathbf{q}/2}|^2}{h^2} - \frac{u_1(\mathbf{0})}{2} \int_{\mathbf{k}} \frac{|\Delta_{\mathbf{k}}|^2}{h^2} \tag{48}$$

The first two terms raise the energy, while the last term lowers the energy of our variational state with respect to the fully valley polarized state. If both bands had the same Chern number, a spatially uniform Δ is allowed so that $\Delta_{\mathbf{k}} = \Delta_0 \forall \mathbf{k}$. In this case, the first term in Eq. (48) does not contribute, and we have

$$e^{HF}(1, \Delta_0) - e^{HF}(1, 0) = \frac{|\Delta_0|^2}{2} \int_{\mathbf{q}} (u_1(\mathbf{q}) - u_1(\mathbf{0})) \tag{49}$$

For a uniform exciton condensate with a spatially uniform Δ , we have $\Delta_{\mathbf{k}} = \Delta_0 \forall \mathbf{k}$. Therefore,

$$e^{HF}(1, \Delta_0) - e^{HF}(1, 0) = \frac{|\Delta_0|^2}{2h^2} \int_{\mathbf{q}} (u_1(\mathbf{q}) - u_1(\mathbf{0})) \tag{50}$$

Since the Landau level projection adds a factor of $e^{-\mathbf{q}^2 l_B^2/2}$ to the bare anisotropy, we have $u_1(\mathbf{q}) < u_1(\mathbf{0}) \forall \mathbf{q} \neq \mathbf{0}$. This negative difference in energy density precisely corresponds to the instability of the fully valley polarized phase of the conventional QHFM to uniform intervalley coherence when $u_1(\mathbf{q}) > 0$. However, for *any* vortex lattice structure, necessitated by topological constraints of hybridizing opposite Chern bands, we have $\Delta_{\mathbf{k}}$ which is a function of \mathbf{k} . Therefore, when u_1 is sufficiently small compared to u_0 the vortex lattice state has a higher energy than the parent insulator, regardless of the exact nature of the microscopic interactions (as long as both are repulsive). This implies that the fully valley polarized state is robust to the vortex lattice phase.

We now carry out the previous analysis for the unpolarized metal, the second state of our interest. In this case, $P_v = 0$ (obtained by setting $h = 0$), so the covariance matrix is given by

$$P_{\tau\tau'}(\mathbf{k}) = \frac{1}{2} \begin{pmatrix} \Theta_{\mathbf{k},\alpha} + \Theta_{\mathbf{k},\beta} & e^{i\phi_{\mathbf{k}}}(\Theta_{\mathbf{k},\alpha} - \Theta_{\mathbf{k},\beta}) \\ e^{-i\phi_{\mathbf{k}}}(\Theta_{\mathbf{k},\alpha} - \Theta_{\mathbf{k},\beta}) & \Theta_{\mathbf{k},\alpha} + \Theta_{\mathbf{k},\beta} \end{pmatrix} \tag{51}$$

In this case, the HF energy density evaluates to

$$\begin{aligned}
e^{HF}(0, \Delta_0) &= \int_{\mathbf{k}} \varepsilon_{\mathbf{k}} (\Theta_{\alpha, \mathbf{k}} + \Theta_{\beta, \mathbf{k}}) - \frac{1}{2} \int_{\mathbf{q}, \mathbf{k}} \frac{u_0(\mathbf{q}) + u_1(\mathbf{q})}{2} (\Theta_{\alpha, -} + \Theta_{\beta, -}) (\Theta_{\alpha, +} + \Theta_{\beta, +}) \\
&= \frac{1}{2} \int_{\mathbf{q}, \mathbf{k}} \frac{u_0(\mathbf{q}) - u_1(\mathbf{q})}{2} \cos(\phi_+ - \phi_-) (\Theta_{\alpha, -} - \Theta_{\beta, -}) (\Theta_{\alpha, +} - \Theta_{\beta, +})
\end{aligned} \tag{52}$$

where the labels \pm are shorthand for momenta $\mathbf{k} \pm \mathbf{q}/2$. We observe that at a total filling of $\nu = 1$, the Fermi surface of the β band is identical to the Fermi surface of the α band shifted by $\mathbf{Q} = (\pi, \pi)$. To prove this, we use $\varepsilon_{\mathbf{k}+\mathbf{Q}} = -\varepsilon_{\mathbf{k}}$ and $\Delta_{\mathbf{k}+\mathbf{Q}} = -\Delta_{\mathbf{k}}$ (as can be seen from the analytical form of $\Delta_{\mathbf{k}}$ in Eq. (35)).

$$E_{\alpha, \mathbf{k}+\mathbf{Q}} = \varepsilon_{\mathbf{k}+\mathbf{Q}} + |\Delta_{\mathbf{k}+\mathbf{Q}}| = -\varepsilon_{\mathbf{k}} + |\Delta_{\mathbf{k}}| = -E_{\beta, \mathbf{k}} \implies \Theta(E_{\alpha, \mathbf{k}+\mathbf{Q}}) = \Theta(-E_{\beta, \mathbf{k}}) = 1 - \Theta(E_{\beta, \mathbf{k}}) \tag{53}$$

This has the very important consequence that the chemical potential μ is fixed to zero at half filling, and the system behaves like a compensated semi-metal with equally sized electron and hole Fermi surfaces. To analyze the energetics,

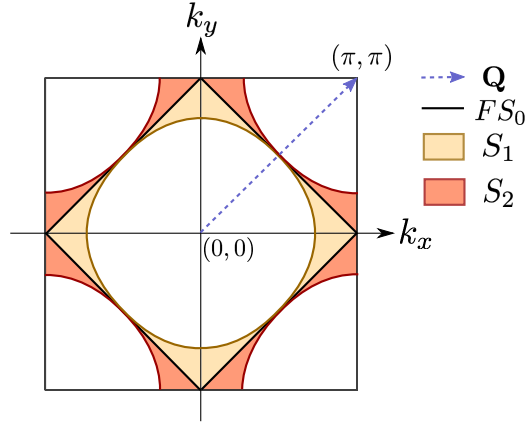


FIG. 6: Fermi surfaces of the α and β bands when $\Delta_{\mathbf{k}} \neq 0$, and the regions S_i which correspond to their differences with the original Fermi surface FS_0 .

it is convenient to define two subsets of the BZ. Let FS_0 be the original diamond shaped Fermi surface of the bands at $\Delta_{\mathbf{k}} = 0$, defined by the contours $|k_x \pm k_y| = \pi$ in the first BZ. Then we define (see Fig. 6)

$$S_1 = \{\mathbf{k} : \mathbf{k} \in FS_0 \text{ and } E_{\alpha, \mathbf{k}} > 0\}; \quad S_2 = \{\mathbf{k} : E_{\beta, \mathbf{k}} < 0 \text{ and } \mathbf{k} \notin FS_0\} \quad (54)$$

Note that $\mathbf{k} \in S_1$ implies $\mathbf{k} + \mathbf{Q} \in S_2$, so the area of S_i ($i = 1, 2$) in the BZ, which we denote by \mathcal{A}_{S_i} are equal. Using these, we compute the kinetic energy term of the vortex lattice phase.

$$\begin{aligned} \int_{\mathbf{k}} \varepsilon_{\mathbf{k}} (\Theta_{\alpha, \mathbf{k}} + \Theta_{\beta, \mathbf{k}}) &= \int_{\mathbf{k}} \varepsilon_{\mathbf{k}} (\Theta_{\mathbf{k} \in FS_0} - \Theta_{\mathbf{k} \in S_1} + \Theta_{\mathbf{k} \in FS_0} + \Theta_{\mathbf{k} \in S_2}) \\ &= 2 \int_{\mathbf{k} \in FS_0} \varepsilon_{\mathbf{k}} + 2 \int_{\mathbf{k} \in S_2} \varepsilon_{\mathbf{k}} \end{aligned} \quad (55)$$

The second term is positive, and denotes the increase of kinetic energy of our variational state by virtue of distorting the bands. The interaction term can also be analogously split into contributions coming from the original Fermi surface, and those coming from Fermi surface distortions. Further, we need to consider the overlap of Fermi surfaces shifted by a momenta of \mathbf{q} , but the Landau level projection factors imply that only the overlap at $q \approx 0$ is important when $a \ll l_B$. While our lattice has $a/l_B = \frac{1}{\sqrt{2}\pi}$ so we are not strictly in this limit, it is nevertheless instructive to look at, as the Fermi surface overlaps can be succinctly expressed in terms of S_1 and S_2 . Adding all contributions, we finally find that the energy density difference is given by:

$$e^{HF}(0, \Delta_0) - e^{HF}(0, 0) = 2 \int_{\mathbf{k} \in S_2} \varepsilon_{\mathbf{k}} + \frac{2u_1(l_B^{-1})\mathcal{A}_{S_1}}{l_B^2} \quad (56)$$

where we have approximated $u_1(\mathbf{q})$ by $u_1(l_B^{-1})$ to avoid potential singularities at $q = 0$. For weakly anisotropic repulsive interactions, $u_1 > 0$ so both terms raise the energy of the vortex lattice variational state with respect to the unpolarized metal. For $u_1 < 0$, the first term raises the energy while the second one lowers it. However, in both cases for a small enough u_1 , the vortex lattice state still has a higher energy and will not be favorable.

VI. NUMERICAL HARTREE-FOCK ANALYSIS OF MAGIC ANGLE GRAPHENE

To confirm that the physical picture discussed in the main text in terms of a Lowest Landau model indeed applies to magic angle graphene, we have numerically solved the Hartree-Fock self-consistency equations in the case where there is a sublattice splitting of 15 meV on the top graphene layer. We used a dual gate-screened Coulomb potential with a gate distance of 20 nm, and a dielectric constant of $\epsilon = 9.5$. The twist angle was $\theta = 1.05^\circ$. The simulations were done on a 24×24 momentum grid, keeping six BM bands per spin and valley. The setup of the simulation is exactly the same as that in Ref. [81], and we refer to that paper for more details. We would like to point out that the only assumption that went into the numerics is that the ground state does not break translation symmetry at the Moire scale – every other type of symmetry breaking is allowed to occur and no bias is introduced.

In Fig. 7, we show the self-consistent Hartree-Fock insulating band spectrum at charge neutrality. It has a large bandgap of ~ 30 meV. The four lowest conduction bands, which are the bands we focus on in the main text, also

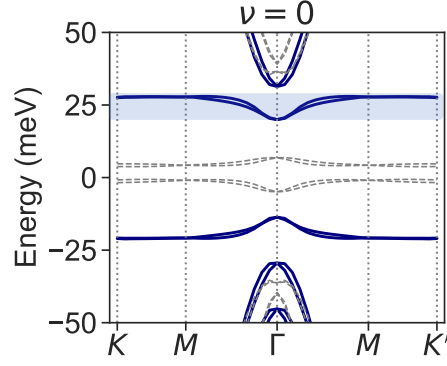


FIG. 7: Self-consistent Hartree-Fock band spectrum of twisted bilayer graphene with sublattice splitting $\Delta_t = 15$ meV and twist angle $\theta = 1.05^\circ$ at charge neutrality (i.e. $\nu = 0$). The active conduction bands, which are approximated by LLL in the main text, are highlighted. The dashed gray lines is the original BM band spectrum.

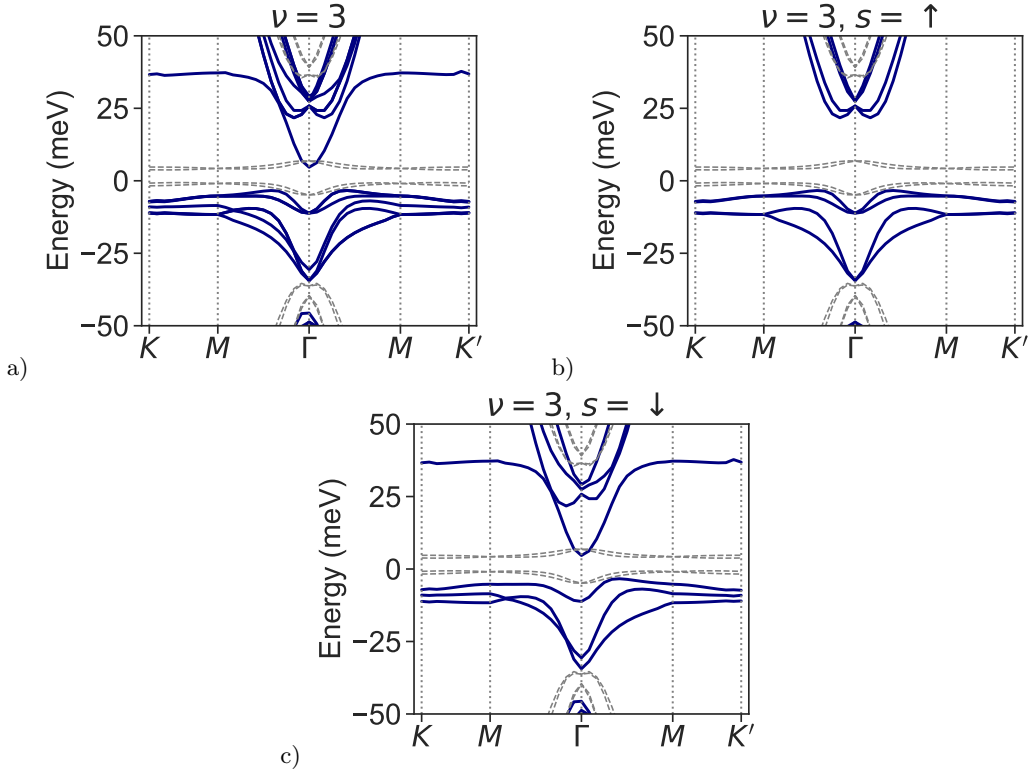


FIG. 8: (a) Self-consistent Hartree-Fock band spectrum of twisted bilayer graphene with sublattice splitting $\Delta_t = 15$ meV and twist angle $\theta = 1.05^\circ$ at $\nu = 3$. The dashed gray lines is the original BM band spectrum. (b) The same as in (a), but only the bands with spin up are shown. (c) Only the bands with spin down are shown.

remain very flat and do not touch the remote bands. The bandwidth is of the same order as that of the bare BM bands. We also find that at charge neutrality, no symmetries are broken spontaneously. Also, if we initialize the algorithm with the state corresponding to the insulating ground state of the BM model with sublattice splitting, we find that convergence is achieved after only 5 to 10 iterations, which means that this state is already very close to the self-consistent solution. Therefore, the bands do not change significantly in going from the BM ground state to the self-consistent solution.

In Fig. 8, the self-consistent band Hartree-Fock band spectrum is shown at filling $\nu = 3$. In 8(a), the total band spectrum is shown, while in 8(b) only the spin up bands are shown, and in 8(c) only the spin down bands are shown. Importantly, we find that system has a clear bandgap, and unbroken valley $U(1)$ symmetry. From Fig. 8 we also clearly see that one spin and valley polarized band of the eight bands around charge neutrality remains unoccupied.

This band spectrum therefore agrees with the general physical scenario put forward in the main text.

VII. ORBITAL MOMENT AND VALLEY-ZEEMAN EFFECT

The momentum-dependent orbital moment of electrons in a band labeled by α is given by [68, 69]

$$m_{\alpha,\mathbf{k}} = \frac{e}{\hbar} \sum_{\beta \neq \alpha} \text{Im} \frac{\langle u_{\alpha,\mathbf{k}} | \partial_{k_x} H(\mathbf{k}) | u_{\beta,\mathbf{k}} \rangle \langle u_{\beta,\mathbf{k}} | \partial_{k_y} H(\mathbf{k}) | u_{\alpha,\mathbf{k}} \rangle}{\varepsilon_{\alpha,\mathbf{k}} - \varepsilon_{\beta,\mathbf{k}}}, \quad (57)$$

where $H(\mathbf{k})$ is the corresponding Bloch Hamiltonian with eigenstates $|u_{\alpha,\mathbf{k}}\rangle$ and eigenvalues $\varepsilon_{\alpha,\mathbf{k}}$. This orbital moment couples linearly to the out-of-plane component B^z of the magnetic field via the orbital Zeeman term

$$H_{OZ,\alpha} = - \sum_{\mathbf{k}} m_{\alpha,\mathbf{k}} B^z. \quad (58)$$

The average orbital g -factor reported in the main text is given by

$$g_v = \frac{2}{A_{mBZ} \mu_B} \int_{\mathbf{k}} m_{+, \mathbf{k}}, \quad (59)$$

where μ_B is the Bohr magneton and A_{mBZ} is the area of the mBZ.